Taking Wireless Underground: A Comprehensive Summary

AMITANGSHU PAL*, Temple University, USA
HONGZHI GUO, Norfolk State Unviersity, USA
SIJUNG YANG, University of Illinois at Urbana-champaign, USA
MUSTAFA ALPER AKKAS, Bolu Abant Izzet Baysal University, Turkey
XUFENG ZHANG, Argonne National Laboratory, USA

The tremendous potentials of sensing and communication technologies have been explored and implemented for different remote event monitoring applications over the last two decades. However, the applicability of sensing and communication technologies do not necessarily limited to above-ground environments, but also implementable and applicable for subterranean, underground scenarios. However, as opposed to air medium, underground communication medium is quite harsh due to the presence of heterogeneous underground materials along with underground aqueous components. In this paper, we provide a technical overview of different underground wireless communication technologies, namely radio, acoustic, magnetic and visible light, along with their potentials and challenges for several underground applications. We also lay out a detailed comparison among these technologies along with their pros and cons using some experimental results.

CCS Concepts: • **Hardware** → Sensor applications and deployments; Sensor devices and platforms; • **Networks** → Sensor networks;

Additional Key Words and Phrases: Underground communication, Channel Modeling, RF communications, acoustic communications, Magnetic Induction Communications, energy harvesting

ACM Reference Format:
Amitangshu Pal, Hongzhi Guo, Sijung Yang, Mustafa Alper Akkas, and Xufeng Zhang. 2020. Taking Wireless Underground: A Comprehensive Summary. *ACM Trans. Sensor Netw.* 1, 1 (November 2020), 39 pages. https://doi.org/0000001.0000001

1 INTRODUCTION

The key purpose of wireless sensor networks (WSNs) is remote monitoring; however, the monitoring needs are not just limited to terrestrial applications but also finds various monitoring needs under the ground. For example, a comprehensive monitoring of soil requires sensing and communications modules buried deep into the soil so that they can sense the conditions near the roots and communicate them without being disturbed by normal tilling/weeding operations. This calls for non-intrusive communications mechanisms that work well with the soil material. In particular, installing antennas that stick out of the ground for in-air wireless communications is both expensive and intrusive. On the other hand, in-ground antennas may not propagate the signals well depending on the wireless technology and soil material. This is just a representative

*This is the corresponding author

Authors' addresses: Amitangshu Pal, Temple University, 1925 N. 12th Street, Philadelphia, PA, 19121, USA, amitangshu.pal@temple.edu; Hongzhi Guo, Norfolk State Unviersity, 410H RTC, 700 Park Ave, Norfolk, VA, 23504, USA, hguo@nsu.edu; Sijung Yang, University of Illinois at Urbana-champaign, 1308 W. Main St. Urbana Illinois, IL, 61801, USA, syang103@illinois.edu; Mustafa Alper Akkas, Bolu Abant Izzet Baysal University, Bolu, 14280, Turkey, alperakkas@ibu.edu.tr; Xufeng Zhang, Argonne National Laboratory, 9700 S. Cass Avenue, Lemont, IL, 60439, USA, xufeng@anl.gov.

1550-4859/2020/11-ART $15.00
https://doi.org/0000001.0000001

example of many such applications that need underground remote monitoring, such as mining, seismic activity etc.

However, underground wireless sensor networks (UWSNs) bring a number of challenges that are unique as compared to the above-ground environment, mainly due to the complex underground environment consists of heterogeneous materials like rocks, sands, clay etc., limited communication range and hard energy supplement. Fig. 1 shows 12 classes of soil textures, having a mixture of clay, silt, and sand with different proportions, as provided by United States Department of Agriculture (USDA) classification [1]. Other than these materials, underground medium also contains water, which absorbs the electromagnetic (EM) wave propagation through the soil. Also different soil textures have different water-holding capacity, which affects the EM propagation.

Radio frequency (RF) based communications are well-researched and work well in above-ground, open, uncluttered environments. However, RF cannot penetrate well in underground cluttered environment, and thus can only work up to certain burial depths. Reducing signal absorption can be achieved by using lower frequencies, but requires bigger antennas. RF is also sensitive to underground water content. RF propagation also varies depending on the soil types; for example RF experiences lesser loss in highly porous soil, whereas higher loss is experienced in compact and watery soil.

Acoustic communication is another promising technology in underground environments, and works well aqueous media. However, the low speed of sound and multi-path effects makes the communication challenging in uncluttered underground environment. Visible light communication (VLC) has recently emerged as a promising technology and works well for underwater communication, but the performance of VLC also deteriorates in cluttered environments.

Another promising and emerging technology is Near Field Magnetic Induction (NFMI or simply MI) based communication. MI communication is based on the principle of resonant inductive coupling (RIC), where two matched coils having an LC circuit communicate with the same resonance frequency. In MI communication the modulated magnetic field by a transmitter forms the basis for near field communications between the transceivers. As the communication is purely magnetic, it does not suffer from usual fading and diffraction effects of the EM communication. Because of these advantages, MI communication can be suitable for near-field underground communication. However, MI signal attenuates very fast, and thus the transmission range is relatively limited.

In this paper we provide a detailed overview of different technologies for underground communication, along with their challenges and applicability. As the topic is quite broad in nature, quite few surveys are studied in the literature. For example, the survey in [2] is a comprehensive review of magnetic induction communication in underwater environments. Although both the underground and underwater environments are different from terrestrial environments, the underground environment has unique characteristics that require radically different design from its counterpart in underwater. Similarly, the survey in [3] and [4] focus on underwater communications and biomedical application, respectively. Because of different scopes, these papers do not include some important works in underground sensor networks. In [5], various communications in underground mines are introduced, including wired and wireless techniques; however, the authors have mainly discussed different radio communication technologies in the wireless context. Although there are some survey articles in the literature that discuss underground magnetic communication [6, 7] separately, we provide detailed comparison of these different technologies using simulations and experimental results to compare and contrast, which makes this paper different than a general survey article. Reference [8] is most relevant to our discussion; however, the article does not provide experimental comparison of different of different technologies. We also discuss some prototype development and discussion for each technology, which are sparse in the other surveys.

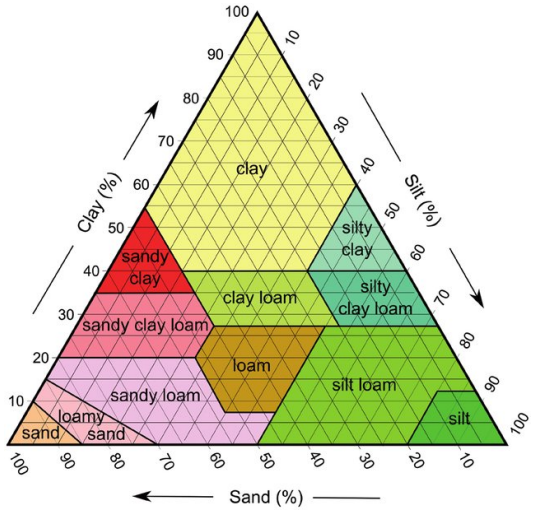

Fig. 1. Different soil types by clay, silt, and sand composition as used by the USDA [1].

The outline of the paper is as follows. Section 2 discusses several applications areas where the underground communication technology is attractive. Section 3–5 extensively summarizes several research achievements of RF, acoustic and MI communication in underground environments. Surveys on VLC are discussed briefly in section 6. Comparison of different technologies along with relevant discussions are summarized in section 7. The paper is concluded in section 8.

2 DIFFERENT USE CASES OF UNDERGROUND COMMUNICATION

Underground wireless sensor networks (UWSNs) has potential applications in several domains, spanning from precision agriculture to underground mine/reservoir monitoring where continuous monitoring of several underground parameters are needed. Below we discuss some of the major applications of UWSNs.

Precision agricultural monitoring: Deploying UWSNs can greatly benefit the agricultural landscape in various ways, spanning from water efficient irrigation control, monitoring the fertility levels of the soils, tests and disease control etc [9]. Recently many parts of the world are experiencing a rapid depletion in ground water levels, which increases the necessity of advanced systems to use the water efficiently for irrigation. Micro-irrigation techniques can achieve this by delivering just the right amount of water to each small area of the agriculture field based on the characteristics of the soil, moisture level, and needs/condition of the plant in that area. This requires burying sensors in the ground close to the plant roots, collecting the data periodically (e.g., once a day), and doing some analytics to determine the irrigation needs [10, 11].

Another important usage of UWSNs is the controlled use of fertilizers both for optimal plant growth and also to minimize waste of fertilizers, since any excess fertilizers end up in the waterways and ultimately in the oceans, causing algae blooms and other problems. Optimal fertilizer application requires automated sensing of soil nutrients like Nitrogen, Potassium, pH close to the plant roots, which requires online monitoring of these parameters using underground sensing nodes.

Underground mines monitoring: The fatality rate of underground mine workers are quite high; according to a report in 2007 the rate is 21.4 per 100k full-time workers in United States [12]. These miners have to work in hazardous environments under the mines, where accidents like rock-bursts, fire, explosion, floods etc. which lead to the collapse of the tunnels wall. In case of

these accidents, these workers are sometimes trapped for several days; one prominent example is the incident of 2006 Sago Mine accident in Virginia, where 12 miners were trapped due to an underground explosion, and many of them had died due to carbon-monoxide poisoning [13]. Another example is the incident of 33 trapped Chilean miners in 2010 who were finally rescued after 69 days [14].

Typically underground mines are monitored with wired, through-the-earth based monitoring and communication infrastructure. In the event of some kind of accident, such as rockfall or explosion, such wired communication breaks down, which leads to complete disconnection of the miners working underground. Such damage of communication infrastructure often makes the rescue works difficult. Thus a wireless underground through-the-rock communication system among the underground miners and the above-ground safety personnel can greatly help the rescue operations in the event of such disasters [12].

Landslide monitoring: Landslide are short-lived, destructive phenomenon, that are caused due to steep slope angle, toe cutting, and saturated soil [15]. In India, on landslide causes an annual damage of $400 million average. The key features of landslides include soil moisture, pore pressure, soil vibration and temperature. The devices need to be buried underground to take these samples and report them to a centralized station. Soil moisture sensors are needed to measure or permittivity of the soil. As rainfall increases, rain water accumulates in the pores of the soil, exerting a negative pressure which causes the loosening of soil strength, which can be measured by vibrating wire piezometer or strain gauge type piezometer [15]. The vibrations caused by the landslides are measured using geophones, whereas the soil temperature can be measured by the temperature sensors to detect a significant anomaly. Since the monitoring devices need to be buried, information exchange among these underground nodes are essential for the continuous monitoring and reporting of these physical parameters.

Poaching detection: Unlawful killing of wild animals or wild plants are crucial for wildlife preserve and maintenance. Especially in Africa and Asia, poaching is becoming a very serious issue with the recent increase in the cost and desire for both ivory and the black rhinoceros horn [16]. The African black rhinoceros, are critically endangered because they have decreased by 80% in the last three rhino generations [17]. Similar to rhinoceros, African elephants, tigers etc. are also heavily threatened by poaching. In fact the elephant population is shrinking with almost 8% per year continent-wide [18, 19]. The poacher detection sensors include video, audio as well as some load sensors that are placed beneath the ground. Such underground load sensors identifies the signature of the poachers and can alert the respective authorities about their activities, for which a wireless communication from underground to above-ground stations are needed.

Underground wildlife monitoring: Habitat monitoring was one of the main application areas of wireless sensor networks, however the work on underground habitat monitoring is relatively sparse. Several species like platypus, badgers etc. dig underground tunnels for their living, thus, tracking subterranean movements, behaviour and habit is quite useful to the zoologists [20]. However, such continuous tracking of their movements and behaviour requires periodic communication from the wireless nodes placed in top of these animal species to the above-ground data collection centers.

Underground mine/reservoir monitoring: Environmental monitoring of underground tunnels spanning several tens of kilometers are crucial for ensuring safe working conditions of the miners [21]. Such applications requires monitoring of the air quality, amount of different gases, dusts etc. under these tunnels. Similarly a real-time and in-situ reservoir monitoring can assist smart drilling for oil and gas in these reservoirs. For example, Petroleum is found in porous rock formations in the upper strata of some areas of the Earth's crust [22, 23]. Such extraction requires tremendous amount of information to accurately control the process to avoid environmental

contamination and improve extraction efficiency. Oil or natural gas pipeline leakages also cause significant economic loss and environmental contamination every year. Such applications also need to deploy some sensor nodes underground that communications with a data collection unit located at the well-bore.

Other than these key areas, underground wireless communication from buried geophones can also be useful for notifying the arrival of trains in unattended crossings, or alert the farmers about arrival of animals like elephants in their agricultural fields that can damage the crops [24]. In the following sections we explore different wireless technologies (i.e. RF, acoustic, magnetic, optical) along with their possibilities and challenges for the use of underground communication in details.

3 RF UNDERGROUND COMMUNICATION

The RF propagation through underground soil follows a complex propagation characteristics, because of different materials present in soil such as rocks, clay, tree roots etc. which causes signal diffraction and scattering. Typically the RF propagation model for UWSNs are borrowed from the free-space propagation model while accounting extra losses in soil. Multiple empirical and semi-empirical models are developed in the literature in this regard [25–27]: which can be categorized into (a) one-path channel model, and (b) multi-path channel model.

3.1 One-path channel model – Modified-Friss model for path loss

The one-path channel model assumes a direct propagation path in between the transceivers. This model is borrowed from the propagation characteristics of RF in free space, also known as Friss path loss model [25] named after Danish-American radio engineer Harald T. Friis (1893-1976). The Friss model is extended in the context of underground communication in the literature, while considering the extra attenuation characteristics of RF propagation. In this Modified-Friss model for underground RF propagation, the received power P_r is given by:

$$P_r = P_t + G_t + G_r - L_0 - L_s \tag{1}$$

where P_t is the transmit power, G_t and G_r are the transmitter and receiver gain respectively, and L_0 and L_s are the path loss in free space and the loss caused by the soil medium respectively. The path loss in free space L_0 can be expressed as

$$L_0 = 20\log\left(\frac{4\pi d}{\lambda_0}\right) = 20\log\left(\frac{4\pi df}{c}\right) = -147.5626 + 20\log(df) \tag{2}$$

where λ_0 is the wavelength in free space and is given by $\lambda_0 = \frac{c}{f}$ where c is the speed of light and f is the operating frequency in Hz.

On the other hand, L_s composed of two components: (a) the transmission loss L_α loss due to the attenuation with an attenuation constant of α, and (b) attenuation loss L_β, which happens due to the different of signal wavelength in soil (λ) as compared to that of free space (λ_0), i.e.

$$L_s = \underbrace{L_\alpha}_{\text{Transmission loss}} + \underbrace{L_\beta}_{\text{Attenuation loss}} \tag{3}$$

This model is also called single path loss or one-path loss model, as it only considers the direct signal between the transceivers. The transmission loss L_α can be expressed as

$$L_\alpha = 20\log|e^{\alpha d}| \approx 8.69\alpha d \tag{4}$$

The attenuation loss L_β can be expressed as

$$L_\beta = 20\log\left(\frac{\lambda_0}{\lambda}\right) = 20\log\left(\frac{c\beta}{2\pi f}\right) \approx 154 + 20\log(\beta) - 20\log(f) \tag{5}$$

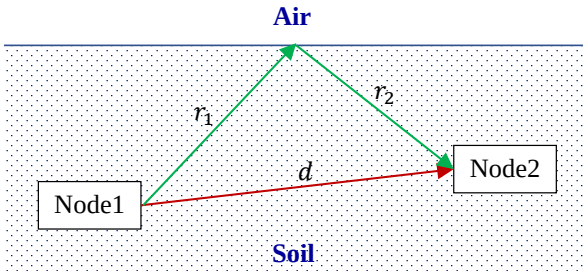

Fig. 2. Illustration of the two-path loss model.

where $\lambda = \frac{2\pi}{\beta}$ and β is the phase shifting constant.

Combining equations(2)-(5), the total path loss in soil medium can be expressed as

$$L_t = L_0 + L_s = L_0 + L_\alpha + L_\beta \approx 6.4 + 20\log(d) + 20\log(f) + 8.69\alpha d \tag{6}$$

Thus the total path loss L_t is a function of (a) the distance d in between the transceivers, (b) the attenuation constant α, and (c) the phase shifting constant β. The parameters α and β depend on the dielectric properties of the soil, and can be expressed as

$$\begin{aligned}\alpha &= \omega\sqrt{\frac{\mu\varepsilon'}{2}\left[\sqrt{1+\left(\frac{\varepsilon''}{\varepsilon'}\right)^2}-1\right]} \\ \beta &= \omega\sqrt{\frac{\mu\varepsilon'}{2}\left[\sqrt{1+\left(\frac{\varepsilon''}{\varepsilon'}\right)^2}+1\right]}\end{aligned} \tag{7}$$

where $\omega = 2\pi f$ is the angular frequency, μ is the relative magnetic permeability, ε' and ε'' are the real and imaginary part of the dielectric constant. Using Peplinski's principle [28] ε' and ε'' can be expressed as [29]:

$$\begin{aligned}\varepsilon' &= 1.15\left(1+\frac{\rho_b\varepsilon_s^{\alpha'}}{\rho_s}+m_v^{\beta'}{\varepsilon'_{fw}}^{\alpha'}-m_v\right)^{1/\alpha'}-0.68 \\ \varepsilon'' &= \left(m_v^{\beta''}{\varepsilon''_{fw}}^{\alpha'}\right)^{1/\alpha'}\end{aligned} \tag{8}$$

where m_v is the water volume fraction in the soil, ρ_b is the bulk density, $\rho_s = 2.66 g/cm^3$ is the density of the solid soil particles, and $(\varepsilon'_{fw}, \varepsilon''_{fw})$ are the real and imaginary components of free water dielectric constant. The expressions α', β', β'' are empirically determined as:

$$\begin{aligned}\alpha' &= 0.65 \\ \beta' &= 1.2748 - 0.519S - 0.152C \\ \beta'' &= 1.33797 - 0.603S - 0.166C\end{aligned} \tag{9}$$

where S and C are the fraction of sand and clay respectively.

3.2 Multi-path channel model

Besides the soil attenuation multiple factors such as multipath spreading and fading affect the channel characteristics of underground radio propagation. Below we discuss some channel models that are developed on top of the modified-Friss model, while considering additional factors such as reflection, refraction, fading etc.

Two-path channel model extension of Fresnel model: The two-path channel model is based on the fact that, if the nodes are buried in an area close to the ground surface, some of the EM waves are reflected back from the ground as shown in Fig. 2. While the direct path in between the transceivers constitute the main component, the reflected path also affect the signal, although it's effect fades with the increase in burial depth of the transceivers. To consider the ground surface reflection, the total path loss is modelled as a combined effect of direct signal component, as well as the reflected component, which can be modeled as [29, 30]:

$$L_f = \underbrace{L_s}_{\text{Single-path loss}} - \underbrace{10 \log V}_{\text{Reflection effect}} \tag{10}$$

where L_s is the path loss due to the single path given in equation (3), and $10 \log V$ is the attenuation factor due to the second path in dB; the term V is given as follows:

$$V^2 = 1 + \Gamma \exp(\alpha \Delta(r))^2 - 2\Gamma \exp(\alpha \Delta(r)) \tag{11}$$

$$\times \cos(\pi - (\phi - 2\pi f \Delta(r)/\lambda)) \tag{12}$$

where Γ and ϕ are the amplitude and phase angle of the reflection coefficient at the reflection point, whereas $\Delta(r) = r_1 + r_2 - d$, (shown in Fig. 2) is the difference of the two paths and α is the attenuation constant.

Even if the two-path model considers the key propagation characteristics of underground RF propagation, inhomogeneous soil characteristics, impurities in the soil, uneven soil surface etc. cause additional scattering, diffraction and fading. To model this, the authors in [29, 30] have extended the two-path model while considering the effects of multipath fading. The concept of multipath fading has been investigated for RF propagation in free space or air. As the multipath channel characteristics obeys Rayleigh (or log-normal probability distribution), each path in the underground channel is assumed to be Rayleigh distributed in [29, 30]. Accordingly the two-path model has been extended by assuming that the received signal is the sum of two Rayleigh fading signals.

CRIM-Fresnel model for path loss: In [26] the authors have developed a semi-empirical path loss model for hybrid wireless underground sensor network, which consist of some underground sensing devices and above-ground router devices for data gathering. Thus the transmission between the sensing devices and the router occurs *partially* through the soil which causes signal attenuation. The authors have developed a path loss model in this scenario by (a) considering the losses due to reflections at the soil-air surface, and (b) developing a Complex Refractive Index Model (CRIM) for estimating the complex permittivity of the soil from the permittivity of solid, water and air. To approximate the signal attenuation from the underground sensing devices to the above ground router communications, CRIM-Fresnel model introduces the total attenuation loss A_t as a (a) sum of soil attenuation, and (b) the signal reflection at the soil-air surface, which is given by

$$A_t = \underbrace{\alpha_c d}_{\text{Soil attenuation}} + \underbrace{R_c}_{\text{Reflection}} \tag{13}$$

where α_c is the soil attenuation (dB/meter), d is the soil depth (meter), and R_c is the attenuation due to reflection. The soil attenuation α_c can be expressed as [26]

$$\alpha_c = 8.68 \frac{60\pi (2\pi f \varepsilon_o \varepsilon'' + \sigma_b)}{\sqrt{\frac{\varepsilon'}{2}\left\{1 + \sqrt{1 + \left(\frac{\varepsilon'' + \frac{\sigma}{2\pi f \varepsilon_0}}{\varepsilon'}\right)^2}\right\}}} \tag{14}$$

where ε_0 is the dielectric permeability in free space and is equal to 8.854×10^{-12} F/meter, and σ_b is the bulk electric conductivity (S/meter). σ_b can be can be derived from the Rhaodes model [31] as follows:

$$\sigma_b = \sigma_w \left(a\theta^2 + b\theta\right) + \sigma_s \tag{15}$$

where σ_w is the electrical conductivity of the soil water solution, σ_s is the surface conductivity, and θ is the soil water content. a and b are the fitting parameters of this model.

When the transmitted signal traverses from the soil to the air medium, a fraction of its energy is reflected whereas the other fraction is transmitted. The reflection coefficient R is the fraction of the transmitted signal that is reflected by the surface of the soil. The reflection coefficient can be calculated according to the Fresnel's equation as follows:

$$R \approx \left(\frac{1 - \sqrt{\varepsilon'}}{1 + \sqrt{\varepsilon'}}\right)^2 \tag{16}$$

The total attenuation R_c due to reflection at the soil-air surface is given by $R_c = 10 \log\left(\frac{2R}{1+R}\right)$.

Combination of modified Friis model and CRIM-Fresnel model: In [27] the authors have introduced a underground wave propagation model by combining the Friis model and CRIM-Fresnel model, by considering the attenuation due to (a) signal reflection, (b) phase shifting, and (c) refraction. The authors have argued that the phase shifting constant (say $\mathcal{P}$), which is the change in phase per meter along the path traversed by the signal, also affects the signal strength. It is measured in radians/meter.

They have also argued that, if the transmitter is located close to the soil-air surface, then the strong refraction will defocus the signal intensity and will result in signal strength. The attenuating factor due to the angular defocusing K is calculated from the Snell's law as follows [48]

$$\sqrt{\varepsilon_s} \sin\phi_s = \sqrt{\varepsilon_a} \sin\phi_a \quad \therefore \; K = \frac{\partial\phi_s}{\partial\phi_a} = \sqrt{\frac{\varepsilon_a}{\varepsilon_s}} \frac{\cos\phi_a}{\cos\phi_s} \tag{17}$$

where ε_s and ε_a are the dielectric permittivities of the soil and air respectively, and ϕ_s and ϕ_a are the incoming and outgoing angle from the normal vector of the surface respectively.

Thus by taking reflection, phase shifting and refraction into account in equation(6), the modified path loss model is derived as

$$\begin{aligned} L_t \approx \quad & 6.4 + 20\log(d) + 20\log(f) + 8.69\alpha d \\ & + \underbrace{20\log(\mathcal{P})}_{\text{Phase shifting}} + \underbrace{10\log\left(\frac{2R}{1+R}\right)}_{\text{Reflection}} + \underbrace{20\log K}_{\text{Refraction}} \end{aligned} \tag{18}$$

3.3 Other relevant studies and experimental prototypes

Similar channel models are studied and tested in [32–34]. In [32, 33] the authors have studied MHz/KHz band for underground channel characterization. The authors in [34] have explored the propagation characteristics of electromagnetic (EM) waves in the Terahertz band (0.1–120.0 THz) in oil/water mixture and soil medium, however, the communication distance is limited to only few centimeters. Underground radio characterization at 97 MHz to 130 MHz is studied both experimentally and analytically in [35]. In [36] the authors have investigated the effects of soil moisture and soil type on wireless RF channel, and studied a multi-carrier modulation technique by adapting coherence bandwidth changes intrinsic to soil moisture variations. The authors have shown that a data rate in excess of 124 Mbps are possible for distances up to 12 m. The impact

Table 1. Representative Studies of RF Ungerground Communication

Types	Key points	Representative Works	Details
One-path channel model	• Assumed direct propagation of radio waves in between the transceivers • Extension of Friss path loss model	Reference [29, 30]	Models transmission loss and attenuation loss
		Reference [32, 33]	Developed the propagation model based on Hertz vector analysis
		Reference [34]	Explored characteristics of EM waves in the Terahertz band, considered oil/water mixture and soil medium
Multi-path channel model	Models EM waves that are reflected back from the ground surface, while considering additional factors such as refraction, fading, scattering etc.	Reference [29, 30]	Modeled reflection at soil surface, multi-path fading
		Reference [26]	Developed a complex refractive index model named CRIM-Fresnel model
		Reference [27]	Combined Friis model and CRIM-Fresnel model, considered signal reflection, phase shifting, and refraction
Experimental validation works		Reference [35]	Studied underground radio characterization at 97 MHz to 130 MHz
		Reference [36]	Studied soil moisture and soil type on wireless RF channel, effect of multi-carrier modulation
		Reference [37]	Studied impact of normalized RMS delay spread on digital modulation techniques
Experimental testbeds		Reference [38]	Used MICA2 sensor nodes in MHz band
		Reference [39]	Used MICAz sensor nodes in GHz band
		Reference [40]	Used Synapse RF300 wireless modules at 915 MHz
		Reference [41]	Used Crossbow wireless modules at 2.4 GHz and 433 MHz
		Reference [42]	Studied ultra-wideband (UWB) underground-to-aboveground communication at 3.1–10.6 GHz
		Reference [43]	Studied underground-to-aboveground communication at 2.4 GHz and 433 MHz
		Reference [44]	Used TI CC430 wireless modules at 433 MHz
		Reference [45]	Used CC1120 RF transceiver in MHz band
		Reference [46]	Studied LoRa radio technology at 174 MHz
		Reference [47]	Studied real-time estimation of soil permittivity and moisture level using RF propagation loss and propagation velocity

of normalized RMS delay spread on the different digital modulation techniques has been studied in [37].

Different experimental testbeds are developed in [38–41]. In [38] the authors have used MICA2 sensor nodes [49] operating in MHz band, where the authors in [39] have used MICAz sensor nodes [50] in GHz band. The authors in [40] have used the Synapse RF300 wireless [51] operating on 915 MHz frequency band. WSN nodes from Crossbow operating at 2.4 GHz and 433 MHz are used in [41]. The impact of soil attenuation on 3.1–10.6 GHz ultra-wideband (UWB) underground-to-aboveground communication is studied experimentally in [42]. Similar underground-to-aboveground communication at 2.4 GHz and 433 MHz is studied in [43]. The authors have investigated the buried antenna orientation, burial depth and soil moisture levels on soil attenuation. The effect of LoRa

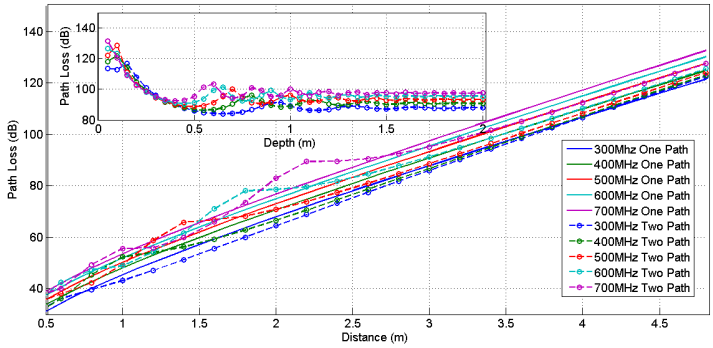

(a) Path loss with different transceiver distances and burial depths

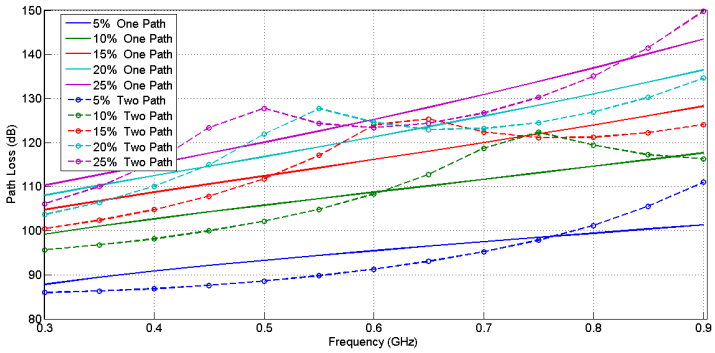

(b) Path loss of one-path and two-path model according to water volume fraction

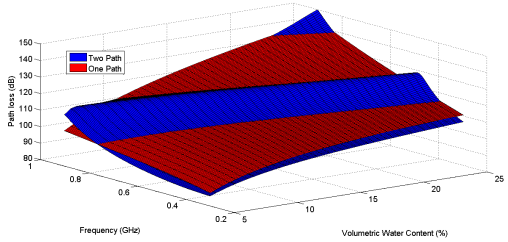

(c) Path with water volume fraction and frequency

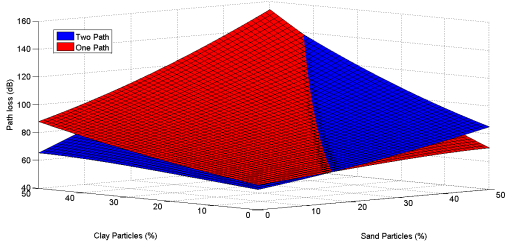

(d) Path loss according to slay and sand particles

Fig. 3. Performance of RF path loss in one-path and two-path model.

(long range) radio technology operating in 174 MHz frequency range is studied in [46]. Similar link quality characterisation of RF underground channel is studied in [44, 45]. In [47] the authors have used the underground RF propagation loss, wave propagation velocity for estimating the real-time estimation of soil permittivity and moisture level in an experimental setting. Different representative works on RF underground propagation is summarized in Table 1.

3.4 Understanding the underground RF characteristics through simulations and measurements

We also highlight the key propagation characteristics of RF channel in underground environments through both simulation studies along with experimental prototyping. The results and outcomes are summarized to validate the primary underground effects of signal attenuation.

Simulation studies of one-path and multi-path channel model: To demonstrate the effect of signal reflection at the underground surface, we have conducted some simulation studies to compare the one-path and two-path channel model. The purpose of demonstrating these two-path channel model is to summarize the effects of reflections and how such reflections matter with different the burial depths. The effect of multiple communication frequencies and underground water content is also demonstrated. For the simulations we vary the communication frequency in between 300–700 MHz, which is close to the operating range if MICA2 sensor nodes that operates in between 315–916 MHz [49]. Such low frequency are appropriate for underground RF propagation with high attenuation loss, whereas using frequencies lower than 300 MHz increases the antenna size and thus is difficult for practical deployments. The bulk density is assumed to be 1.5 g/cm^3 for such experiments. Unless otherwise mentioned the volumetric water content (VWC)[1] as set to 5%, whereas the sand and clay percent is kept as 50% and 15% respectively.

Fig. 4(a) shows path loss of one-path and two-path channel model with different transceiver distances and burial depth (in case of two-path model). Fig. 4(a) shows that as compared to the one-path channel model, the two-path channel model exhibits some ripples. This is due to the reflection at the ground surface, i.e. when the signal is reflected back from the ground surface, it experiences a phase change. Thus the resultant path lass is a combination of direct signal along with the reflected component, which contributes constructively and destructively in received signal strength. Also notice that the effect of these ripples reduce as the transceiver distance increases beyond 3 meters, as the reflected component becomes weaker with the increase in distance. Fig. 4(a) also shows that the path loss increases with transceiver distance as well as with the increase in frequency.

The inset figure in Fig. 4(a) shows the path loss in between two underground transceivers with different burial depths in case of two-path model. From this figure we can also observe the ripple effects, and thus the loss does not vary homogeneously with the increase in depth. We can also observe that the ripple effect diminishes with the increase in depth due to weaker reflected component. Thus for small burial depths and transceiver distances, the two-path loss model is more accurate, whereas the models behaves almost identical with the increase in distance and depth.

Fig. 4(b) shows, the one-path and two-path channel model while varying the water volume fraction from 5% to 25%. The transceiver distance and burial depth is set to 3 meters. From Fig. 4(b) we can observe that with fixed transceiver distance, the path loss increases with the increase in water volume fraction; this shows the effect that the RF signals are absorbed in underground aqueous medium which increases the loss. The figure also shows some irregular fluctuations of two-path channel model; however, the trend of path loss is consistent with that of one-path channel model.

Fig. 4(c) shows the path loss of one-path and two-path model according to water volume fraction and frequency. As expected, the path loss increases with the increase in frequency and water content. For one-path model this variation is quite consistent and gradual, whereas the two-path model demonstrates a wavy variation because of surface ground reflections. The effect of clay and sand particles on path loss is demonstrated in Fig. 4(d), where the operating frequency is set to 400

[1]The volumetric water content is a numerical measure of soil moisture, which is simply the ratio of water volume to soil volume.

MHz. From this figure we can observe that the path loss increases with the increase in clay and sand particles percentage. Also the variation in two-path model is quite gradual as the distance and burial depth have been remained fixed for Fig. 4(d)

Findings from an experimental prototyping: We also demonstrate the effect of underground RF characteristics from an UWSN testbed developed at the University of Chicago, where 27 underground sensing nodes are deployed with varying burial depths within 6 to 14 inches. The basestation is placed above the ground; the underground nodes record and send periodic moisture levels to the above-ground basestation. The nodes operate at 902 MHz ISM band. The transmit power is set to 22 dBm, which provides a link budget of around 160 dB. The nodes are equipped with Texas Instrument MCU MSP430F5529 chips with the CC1120 RF transceivers, that are enclosed in a water-proof box as shown in Fig. 4(a). Fig. 4(b) shows the spatial variation of RSSI and SNR from the sensor nodes within one square mile area from the basestation. From this figure we can observe that the coverage area is quite large because of lower burial depth and high link budget, which leads to acceptable level of signal-to-noise ratio (SNR). However, the signal strengths from all the sensing points are below -95 dBm, which shows high loss due to underground attenuation.

Fig. 4(c) shows the variation of RSSI and VWC with over the span of one week. From this figure we can observe a strong correlation between the RSSI and VWC, i.e. whenever the soil moisture level increases, the RF absorption increases and thus RSSI starts decreasing and vice versa. This also validates our simulation outcomes in Fig. 3(c). Fig. 4(d) shows the effect of burial depths on the RF path loss, where the sensor nodes placed at different underground depths send their recorded data to the above-ground basestation. From this figure we can observe that the signal experiences high loss of more than 100 dB within 5 inches under the ground, and then fades rapidly within 30 inches. This also validates that the RF communication is only limited within few inches under the ground, and so its application is only limited to such low depth deployment scenarios.

3.5 Key obstacles of RF for underground communication

RF underground communication faces different challenges due to heterogeneous underground medium, along with underground water volume. As demonstrated in our results in Fig. 3, the path loss of radio waves are affected as the ratio of sand, clay and water volume fraction changes. As the sand, clay and water volume fraction changes depending on the soil textures, the communication distance changes as well.

Because of these effects, the communication range may vary due to the seasonal changes, which affect the underground properties. Especially the water volume fraction changes rapidly during the wet and rainy seasons, which causes extra RF absorption and thus changes the communication range and quality. Thus, depending on the soil types, extent of seasonal changes on the soil, and the expected communication range, the designers of UWSNs need to find out the appropriate frequency channels and other design parameters, as we have seen that the propagation characteristics changes quite a bit with the operating frequency. In fact, in underground scenarios, the broken/fault sensors are difficult to be replaced. The challenge is even severe in underground RF communication because of its high path loss, i.e. due to the limited communication range, a small fraction of faulty sensors can disconnect an big fraction of a UWSN.

4 ACOUSTICS BASED UNDERGROUND COMMUNICATION

As observed in the previous section, RF signals suffer from severe attenuation in underground soil medium. Furthermore, their implementation is highly limited by environmental conditions due to their high sensitivity to the water content level in soil; the propagation losses increase as the water content increases [52].

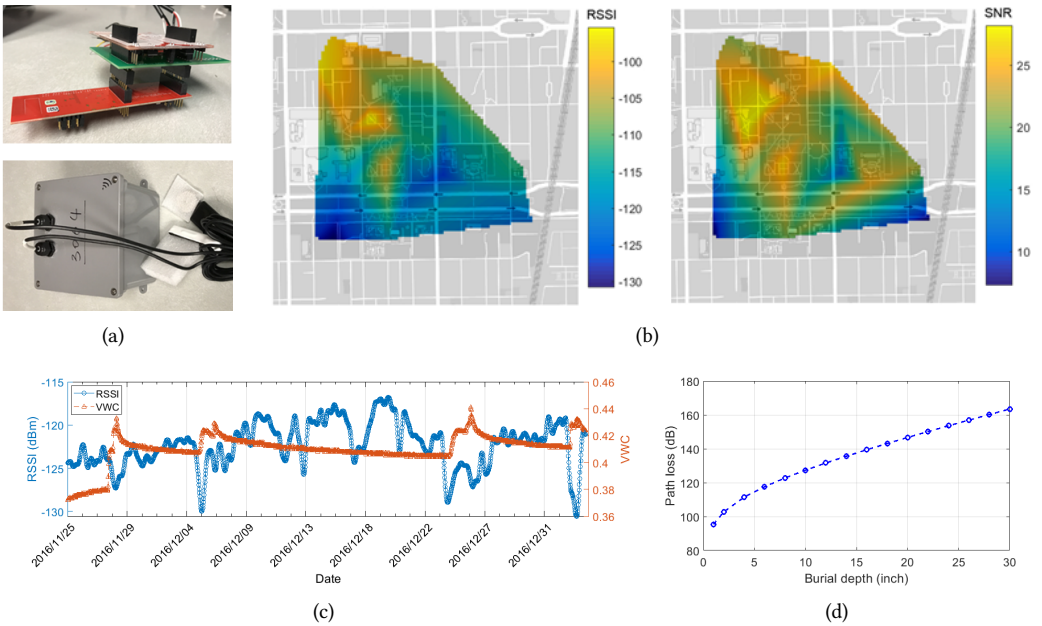

Fig. 4. (a) Transceiver setup inside a box that to be deployed underground, (b) spatial intensity map of RF RSSI and SNR, where each map is of 1×1 sq. mile. (c) The variation of RSSI and VWC by a sensor node, which shows a strong correlation among the two. (d) Variation of path loss with burial depth.

Meanwhile, in recent decades, acoustic communication has been successfully implemented in underwater environments [53–57], where traditional RF communication is similarly limited by extreme path losses. For underground applications, a few of similar approaches have been proposed via acoustic waves propagating through soils.

Development of reliable acoustic communication links among UWNS's requires identifying the soil acoustic channel characteristics, whose propagation models are much more comprehensive than its underwater counterpart. While water only admits pressure waves, soil, a multi-phase inhomogeneous material consisting of both solid particles and fluids, can simultaneously exhibit both kinds of body waves: compressional and shear waves. In addition, body waves interacts with surface layers, producing Rayleigh and Love waves [58].

4.1 Through-soil acoustic channel attenuation model

Attenuation is of major importance to communication problems, since it controls the maximum range over which the signal can be transmitted; the lower the attenuation, the greater the range of transmission that can be achieved. Acoustic attenuation model can be similarly expressed as the RF propagation loss model in (1). Attenuation process can be separated into two types of damping: geometric and material damping. The geometric damping depends on the type and the location of vibration source and increases polynomially with distances. The material damping is related to properties of soil medium and vibration amplitudes, and typically increases exponentially with distances. In result, as the acoustic wave propagates through a soil media, the sound intensity at

distance d, denoted as $P(d)$ decreases from the initial intensity P_0 as

$$P(d) \propto \underbrace{\frac{1}{d^{\gamma}}}_{\text{Geometric}} \underbrace{e^{-\alpha d}}_{\text{Material}}, \tag{19}$$

where α is the attenuation coefficient (in dB/m), and γ typically has a value between 1 and 3, depending on the beam pattern of electroacoustic transceivers.

In soil sediments, three mechanisms are known to cause most of the observed material damping behaviors: scattering, frictional losses at grain-to-grain contacts, and viscous losses from grain-to-fluid motions. Scattering can be caused by grains in various sizes, i.e., when the wavelength of the acoustic wave approaches to the size of each grains which incorporates the soil sediments, scattering loss dominantly occurs. In other words, for most UWSN applications using acoustic means in audible ranges, this type of loss can be safely ignored. Meanwhile, the frictional and viscous losses are usually referred to as intrinsic attenuation, since their occurrences are mostly prevailed by intrinsic materials properties of soil sediments. The observed acoustic properties generally result from all three mechanisms, but, under various conditions for certain sediment types, one or two of the mechanisms may dominate [59]. The total of all losses is called effective attenuation [60], and it has been observed to depend on a host of factors, including plasticity, strain amplitude, mean effective stress, void ratio, loading cycles, grain sizes, degree of water saturation and thixotropic effects [61–67]. Most theories explaining these observed material behaviors generally fall into one of two groups: viscoelastic and physical sediments models.

Viscoelastic models consider the soil medium as a continuum with viscoelastic properties, representing the bulk material as a whole. In these models, acoustic responses are commonly described by complex moduli and relaxation functions, which can be calibrated from observed behaviors. The most well known theories are Kelvin-Voigt, and Hamilton's viscoelastic model [68, 69]. Hamilton's model assumes that sediments can be represented by an isotropic two-phase system composed of solid grains and water. For both compressional and shear waves propagating through soil, the following can be derived from the model:

$$Q^{-1} = \frac{\alpha V}{\pi f - \alpha^2 V^2/(4\pi f)}, \tag{20}$$

where Q^{-1} is the specific attenuation factor, f is frequency, and V is the speed of sound. When energy dissipation is small, or in high frequency ranges, the second term of the denominator in the right side of (20) can be approximately ignored, and the following relationship holds between attenuation and frequency:

$$\alpha \approx \frac{\pi f}{QV}. \tag{21}$$

Therefore, if the specific attenuation factor Q is independent of frequency, the attenuation coefficient α in (19) is linearly proportional to frequency, making the resulting path gain over frequency f and distance d as [70]

$$H(f, d) \propto \frac{1}{d^{\gamma}} e^{-\alpha 2\pi f d} e^{j2\pi f d/c}. \tag{22}$$

Additionally, the specific attenuation factor for compressional waves Q_p and shear waves Q_s can be expressed as

$$Q_p = \frac{\lambda + 2\mu}{\lambda' + 2\mu'} \qquad Q_s = \frac{\mu}{\mu'} \tag{23}$$

where $\mu + j\mu'$ and $\lambda + j\lambda'$ refer complex Lamé elastic moduli of the viscoelastic mateiral. In [62], Hamilton divided the ocean floors into general environments each characterized by a distinctive

sediment type, and assigned averaged parameter values to fit for observed acoustic behaviors of various types of sediments.

Physical sediment models focus more on individual constituents and the structural characteristics of the skeletal frame of the soil. These models can explain how various observed acoustic behaviors can be determined over soil physical properties [60]. Biot-Stoll model [71–74] is the most widely used theory among them, explaining that energy dissipation occurs in two different mecahnisms: frictional losses due to the inelasticity of the sediment skeleton, and viscous losses due to the interstitial fluid. The complex interaction of these mechanisms results in a form of frequency-dependent damping, whose attenuation coefficients depend on soil physical properties such as porosity, grain size, permeability, and the effective stress. However, in acoustic community, the Biot-Stoll model has not been widely accepted to fit and model practical soil acoustic channels due to its complexity; the amount of observed data are not enough to adequately verify the model's prediction. Furthermore, many of effects predicted from the Biot-Stoll model are of relatively small magnitudes compared to typical noises in attenuation measurements.

Therefore, many additional attempts have been made to quantify attenuation coefficients through experimental measures at both fields and laboratories.

Laboratory measurements: In [75], researchers had performed one of the earliest experiments to quantify attenuation in laboratory. The setup was simple: a wooden chamber was coated inside with a cotton blanket and the soil was placed in different thicknesses. A whistle was used as a source and the speakers were placed on the other end of the soil. Acoustic signals were sent, ranged in frequency from 10 to 35 kHz. The moisture level was varied by mixing different amounts of water. The values of attenuation obtained were relatively ranging between 3 dB/cm to 76 dB/cm. When water was added in a way that allowed air bubbles to be trapped in the soil, the attenuation levels were relatively very high, ranging between 56 dB/cm and 71 dB/cm for different frequencies. When vacuum was applied for some hours, eliminating trapped air, the attenuation dropped to around 3 dB/cm. This demonstrated the effect of entrapped air in magnifying attenuation. In [60], researchers stated that the accurate measurement of attenuation requires the specimen to be much larger than the wavelength of the propagating wave, and thus suggests that laboratory measurements are restricted to frequencies of 10 to 20 kHz and above. Below these frequencies, compressional wave can only be studied in the field. In [65, 66] researchers conducted similar laboratory experiments on soils. The samples were chosen to include low and high contents of organic matter, sand, silt and clay, and a range of clay mineralogy. Moisture content ranged from air-dried to saturated. Specimens ranged from loose to compact. The acoustic signal is propagated through the soil sample contained in a tub which is coupled to face of the acoustic source via a water interface. The transmitted acoustic signal is received by a hydrophone which is acoustically coupled to the top of the soil sample with phenylated silicon oil. The attenuation coefficient over the 1-10 kHz were ranged between a low of about 0.1 dB/cm·kHz which was most prevalent for the loose dry samples and a high close to 1 dB/cm·kHz which was most prevalent for the compact samples with more moist.

Field measurements: In [63], researchers measured attenuation characteristics, using geophones, for various sources and soil conditions including residual sandy silt, bedrock, gravel and clay. The sources included ground vibrations induced by two train loading, blasting and steel pipe driving. The material damping for each site and loading condition was calculated and reported. The material damping coefficients of the site with trains were evaluated as 0.02 and 0.008 (1/m). The corresponding damping ratio and the maximum strain amplitude were 2.3 and 0.01% for the first train, and 0.9 and 0.002% for the second train. The material damping coefficient of the site with blasting load was evaluated as 0.026 (1/m). The corresponding damping ratio was 4–5% which was reasonable at a maximum strain amplitude of about 0.01% where the site soil experienced. For the

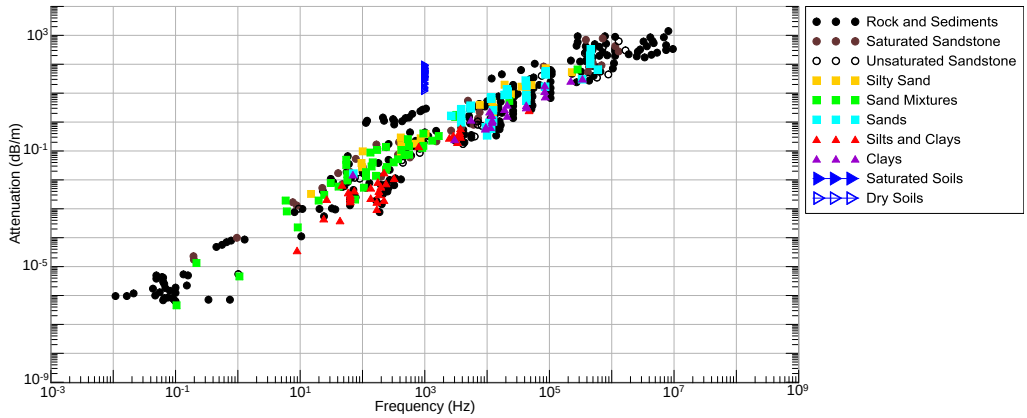

Fig. 5. Acoustic attenuation for different types of soils over a wide range of frequency compiled from [60, 62, 63, 66]

steel pipe driving site, for the far field case, the material damping coefficient of 0.026 and damping ratio of 5 to 6% with a maximum strain amplitude of about 0.001%. The corresponding damping ratio in the near field was about 40% at the strain amplitude of 0.05% and the damping ratio in the far field was about 3% at strain amplitude of about 0.004%. In [60, 62], a lot of attenuation data from field measurements were combined to build a comprehensive data set for marine sediments. Above mentioned data are compiled in Fig. 5. The importance of this figure is that it summarizes a lot of attenuation data for a range of soil types and over a range of frequency ranging from 0.001 Hz and 10 MHz. As can be seen from Fig. 5, the relationship between the frequency and the attenuation coefficient shows approximately a linear trend as expected from equation(21).

Summary of effects of physical parameters on attenuation: In [76], researchers showed that significant compressional attenuation was found in partially saturated rock. In [77], it was concluded that attenuation was clearly sensitive to pressure, the degree of saturation and probably to frequency. In [78], it was shown that the velocities and attenuations in rocks are not constant with frequency. In [66], it was reported that saturation levels in porous materials have been shown to affect the speed and attenuation of compressional and shear waves. The authors claim that increasing the stress in granular materials will typically increase the propagation speed and decrease the attenuation. In their measurements speed was negatively correlated with attenuation and measured water content. Saturated soils showed no significant correlations between attenuation and any soil parameter. However, in unsaturated soils, water content was strongly correlated with attenuation. The authors explain the increase in attenuation as a result of the viscous losses caused by the increase if water in pore space of the soil.

Discussions about nonlinearity observed at lower frequencies has been a subject for debate for a long time. For the practical considerations, this discussion has low significance so it will not be covered in this review.

4.2 Scattering and Multi-path effects

Acoustic waves, being mechanical in nature, scatter whenever they encounter a boundary between two materials, according to Snell's law. That is, if a beam strikes the boundary from material 1 to material 2 at (angle, velocity) given by (θ_1, V_1), it produces (a) a reflected beam at $(-\theta_1, V_1)$

through material 1, and (b) a pass-through or refracted beam at an angle, velocity (θ_2, V_2) such that $V_2/V_1 = \sin\theta_2/\sin\theta_2$ where θ_2 depends on the refractive index of material 2. With many boundaries of irregular shape, the net impact of the scattering on the magnitude of the signal can be described statistically using the Nakagami distribution [79].

As the acoustic signal propagation is slower than electromagnetic propagation, multiple delayed and distorted versions of the transmitted signal arrives at the receiver, which results in a significant amount of inter-symbol interference (ISI). At the same time the low speed not only increases the propagation delay or round-trip time, but also amplifies the Doppler effect. Soil is typically inhomogeneous in nature which also leads to multiple interbed reflections and refractions. The resulting channel frequency response can be represented as [70]

$$H(f) \propto \sum_{i=1}^{M} k_i e^{-\alpha_i \pi f d_i} e^{j2\pi f d_i/c_i} \tag{24}$$

where k_i's refer constant complex gains, whereas α_i, d_i and c_i represent the frequency independent attenuation coefficient, transceiver distance and the speed of the travelling mode of the acoustic signal along each of i-th paths. Using real experiments, the authors in [70] have estimated an acoustic delay spread of 500 ms, at a distance of 25 m at the farm area in Illinois, using a 250W speaker with a 5s long chirp signal from 20-100 Hz. Without an elaborated signal processing scheme, such large delays originated from multipath effects could result in limiting the data rate and bandwidth availability for the underground, through-soil communication. Furthremore, even frequency-selective attenuation from free-space propagation stimulates non-negligible delay spreads.

4.3 Wireless acoustic technologies in soil

Even though soil acoustic channels have potential advantages on longer range applications due to its lower path losses, they had not been discussed seriously as wireless acoustic communication channels till recent years. The first academic attempt to use acoustic or seismic propagation goes back to 60's in [80]. They invented thumping type of transducers to generate and receive 80 Hz analog AM-modulated signals, and utilized them to communicate from a hill top to an underground mine through earth in hundreds of meters range. This work inspired the development of some seismic communication schemes, mostly targeting the remote switching of perforating drills [81, 82]. However, this attempt was limited to transmission of harmonic signals of periods longer than 0.5s, for which a simple communication scheme, such as on-off keying (OOK), may work but would yield extremely low data rates (< 2bps). Furthermore, the transmitting sources used were surface-mounted, making this system only capable of uni-directional downlink applications from an above-ground base station to underground devices; they are not suitable for sensor networks applications, which requires bidirectional connections among fully embedded underground sensors. Additionally, the size of these instruments limits their utility, having pistons larger than 30 cm in diameter.

In [70] the authors have first developed a low-cost, compact through-soil underground acoustic communication system using off-the-shelf tactile speakers and motors. With an acoustic source upto 250 W in average power, experiments was conducted at the testbed implemented at farm areas in Illinois (shown in Fig. 6(a)). It was shown that a maximum communication range of 50 m with a data rate of 2 to 24 bps can be achieved through low frequency (40 Hz) acoustic signals. Also, additional experimental testbed was installed in lab conditions using a metal horse trough, showing achievable data rates upto 2 kbps at a range of 30 cm with 30W acoustic sources. As illustrated in Fig. 6(b), a QPSK modulation schemes was adopted for digital data transmission. Decision feedback

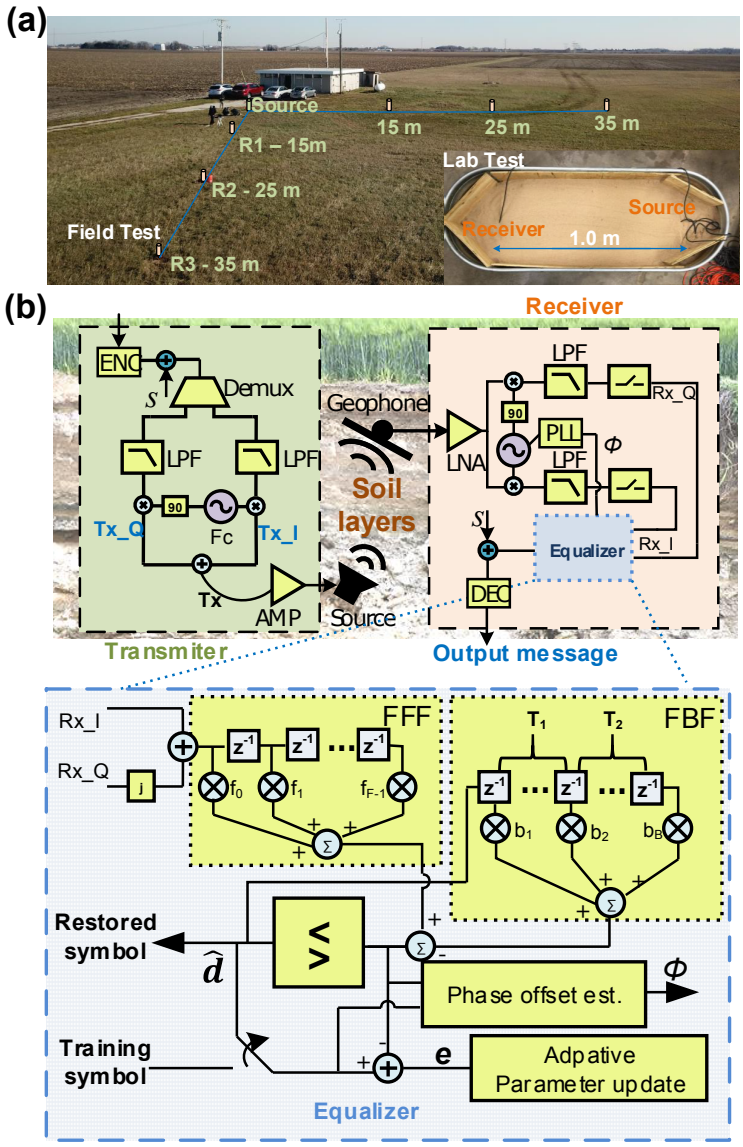

Fig. 6. (a) Photos showing the experimental data transmission setup for through-soil acoustic communication in Champaign, IL, and (b) the schematic of the proposed system in [70]

equalizer (DFE) and phase locked loop (PLL) were exploited to compensate ISI's from dispersive multi-path channel responses and Tx/Rx clock offsets. In [83], the proposed system in [70] has been shown to be capable of remotely receiving values from geotechnical sensors buried in deep bore holes.

Underground acoustic communication can be also used for down-hole telemetry purposes through steel walls of the drill string [85–87]. Though they can be only implemented with the existence of long steel walls connecting Tx/Rx sides, reliable data transmission is achievable for

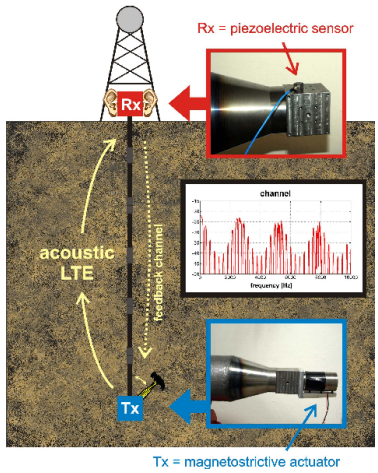

Fig. 7. Acoustic transceivers for down-hole communication [84].

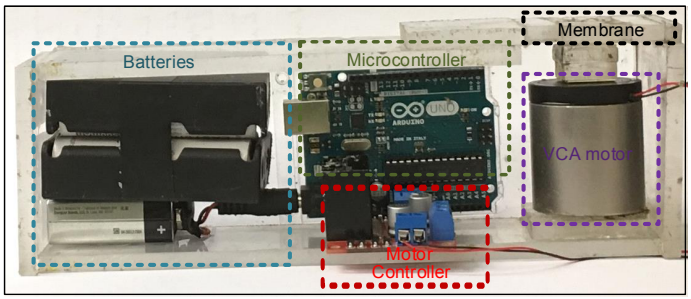

Fig. 8. Acoustic modem prototype proposed in [70] for data transmission through soil

long distances. Such acoustic based telemetry system consists of (a) an underground piezoelectric-electric transmitter, (b) repeaters at 500-2000 m apart, and (c) a transceiver at the ground surface, as shown in Fig. 7. The underground down-hole transmitter encodes the sensory data, convert this to the acoustic signal and propagates to the surface via the metal string. In [88] the authors have experimentally found the attenuation on the drill string ~4-7 dB/1000 feet. In [84, 89, 90] researchers achieved a data rate of 20 kbps at 4.5 m and 6 kbps at 55 m depth. They have used orthogonal frequency division modulation (OFDM) for frequency selective channel along the pipe strings. Single carrier with frequency domain equalization (SC-FDE) is proposed in [92] to improve the reliability of the acoustic communication. In [93] the authors have used ASK/FSK for modulation, whereas trellis coded modulation is explored in [94]. A non-contiguous OFDM scheme is also used in [91] for such down hole communication. Multi-channel acoustic communication through the underground steel wall is also explored in [95]. The authors have also compared the effects of single channel and multi channel acoustic communication in oil wells.

4.4 Challenges and requirements in acoustic modem design

To be reliably employed for WUSN applications, acoustic sources should meet system specifications required for various applications suggested in section II; they should be able to operate at frequencies suitable for soil acoustic channel characteristics and target data rates with a certain constraint on power consumption. Since lower-frequency waves suffer less from the path loss, as illustrated

Table 2. Representative Studies of Underground Acoustic Communication

Types	Key points	Representative Works	Details
Soil propagation modeling and measurement of acoustic behaviors	• Attenuation coefficient is linearly proportional to the frequency of the sound • Viscoelastic and physical sediments models explain the dependency of acoustic properties upon soil physical properties	Reference [60, 62, 68, 69]	Viscoelastic models for through-soil acoustic propagation
		Reference [60, 71–74]	Physical sediments models for through-soil acoustic propagation
		Reference [61–67, 75–78]	Field and laboratory measurements on soil acoustic behaviors
		Reference [70]	Soil acoustic channel model with multipath scattering
Experimental validation/ prototypes		Reference [80]	Develop 80 Hz analog AM-modulated system for underground mines
		Reference [81, 82]	Periodic transmission of acoustic impulses for switching of perforating drills
		Reference [70, 83]	Develop 2-24 bps OOK/QPSK modulated digital transmission upto 50m ranges using low power sources
Down-hole telemetry systems through steel drill walls	• Acoustic communication through steel walls of the drill string • Consists of an underground piezoelectric transmitter, repeaters at 500-2000 m apart, and a transceiver at the ground surface	Reference [85–88]	Characterization and experimental testbed implementation of acoustic channels through underground drill walls
		Reference [84, 89–91]	OFDM based systems for frequency selective channels along underground pipe strings
		Reference [92, 93]	Single carrier based systems with equalization blocks
		Reference [94]	Develop system with trellis coded modulation
		Reference [95]	Explore multi-channel system for underground channel through drill walls

in Fig. 5, and bandwidth requirements for many underground applications are not high, most through-soil acoustic communication systems have adopted sounds in lower frequency ranges.

In addition, wireless nodes for underground applications need to be small enough to fit within underground boreholes, e.g., diameter of a borehole varies upon different purposes, but typically ranges between 2 and 4 inches.

However, common loud speakers that can efficiently deliver such frequencies are necessarily characterized by larger dimensions that exceed typical borehole diameters. For example, a plane circular piston source, a simplified model of most circular loudspeakers, has a far-field beam-width which depends on the diameter D of the source and frequency f. In particular, if β is the half-width angle of the beam, then

$$\sin(\beta) = \frac{0.514c}{fD}, \tag{25}$$

where c represents the speed of the signal through the medium. Thus, to produce a narrower beam, we need a larger diameter and higher frequency. In other words, with a fixed diameter, a narrower beam can only be achieved with higher frequency, which results in higher attenuation.

In [70, 83], authors proposed a prototypical through-soil acoustic modem illustrated in Fig. 8. They bypassed the trade-off relationship between the path loss and the size by adopting voice coil motors (VCM) which generate acoustic spikes for the OOK modulated signal instead of using common loudspeakers. From testbed experiments conducted at farm areas in Illinois, it was reported that the 9W prototype achieves a data rate of 4 bps for a maximum communication range of 10m.

Table 3. Representative Studies of MI Underground Communication

Types	Key points	Representative Works	Details
Channel & antenna model	• Assume the communication range is within the near-field • Use an equivalent circuit model with mutual inductance representing the channel quality	Reference [99]	Path loss model for underground direct MI communication and MI waveguide
		Reference [100]	Channel and antenna models and key parameters optimization
		Reference [101]	Through-The-Earth communication channel model for large devices
Antenna array model	Improve MI communication reliability and data rate by using various antenna array configurations	Reference [102–106]	Develop planar coil arrays and beamforming algorithms
		Reference [23, 107–115]	Develop tri-axis coil array and transmit and receive algorithms
		Reference [116–118]	Develop spherical coil arrays based on metamaterial-inspired approaches
Modulation	Develop signal modulation schemes for MI communication taking into account of the extremely narrow bandwidth and near-field characteristics	Reference [119]	Studied underground digital modulation schemes
		Reference [120]	Studied direct antenna modulation for MI communication to overcome the narrow bandwidth challenge
		Reference [110]	Studied magnetic vector modulation using tri-axis coils
Experimental validation works & testbeds	Design MI communication testbeds using various hardware, such as USRP and microcontrollers	Reference [113, 121]	Use USRP to develop MI communication testbeds and use GNU radio or MATLAB to process wireless signals
		Reference [104, 110–112, 122–124]	Use microcontrollers to design MI communication testbeds. MI communication algorithms such as beamforming, were presented

5 MAGNETIC INDUCTION COMMUNICATIONS

Magnetic induction communication was introduced for wireless communication in the ocean [96]. It also has the potential to work in various harsh environments such as underground and intrabody [97, 98]. In this section, we introduce different concepts of magnetic induction-based communication techniques in underground environments. We first summarize the antenna design, signal processing, network design, and testbed design for magnetic induction communications. Finally, we identify major research problems and challenges. A summary of the representative studies is given in Table 3.

5.1 Magnetic antenna designs

5.1.1 Advantages of Using Magnetic Coils. Compared to electric fields, magnetic fields experience less propagation loss since most of the materials in nature have similar permeability. According to Maxwell's equations, if the frequency is zero, electric fields and magnetic fields are decoupled and they do not affect each other. However, wireless communication requires nonzero bandwidth and relatively high carrier frequency. If the carrier frequency is not zero, electrical fields and magnetic fields are coupled together, and we cannot consider them independently. Nevertheless, this coupling process happens gradually as the distance from the transmitting antenna increases. Hence, in the near field, the electrical fields and magnetic fields are loosely coupled, which can be used for magnetic induction communication. Following the approach in [125], in Fig. 9 we show the wave impedance (the ratio of electric fields over magnetic fields) of electromagnetic fields generated by electrical antennas and magnetic antennas. The distance from the transmitting antenna is scaled

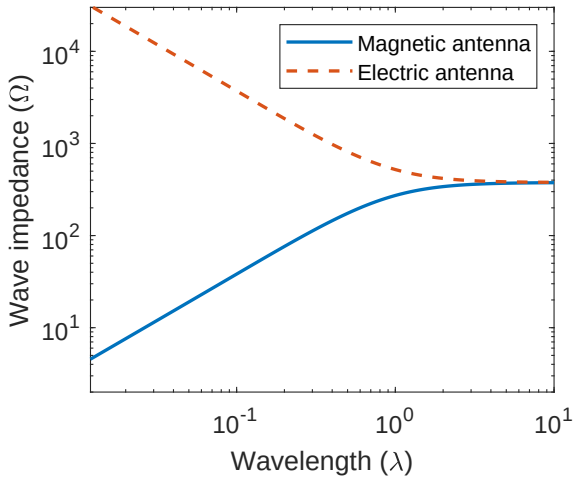

Fig. 9. Wave impedance E/H of electric and magnetic dipoles. The x-axis is the distance from the transmitting antenna that is scaled by the wavelength.

by the wavelength to show the near field better. As we can see, in the near field, i.e., the distance is much smaller than λ, electric antennas generate much more electric fields than magnetic antennas. In the far-field, electric fields and magnetic fields gradually coupled together, and the ratio becomes a constant. If using magnetic antennas, we can obtain more magnetic fields which is desirable for underground communications.

5.1.2 Joint Coil and Channel Model. The magnetic coil is key to achieve the promised performance of magnetic induction communication. Recently, Morag *et. al.* [100] presented a comprehensive coil model considering both the low frequency and high frequency effects, which jointly design the coil to obtain an optimal configuration considering multiple high-frequency and low-frequency constraints. Since the wavelength of magnetic induction communication is much larger than coil size, usually, we can safely consider the coil as an infinitesimal magnetic dipole [126]. The magnetic fields radiated by an infinitesimal dipole in spherical coordinates can be written as

$$h_r = \frac{jka^2 NI_z \cos\theta}{2r^2}\left[1 + \frac{1}{jkr}\right] e^{-jkr}\hat{r}, \tag{26}$$

$$h_\theta = \frac{-k^2 a^2 NI_z \sin\theta}{4r}\left[1 + \frac{1}{jkr} - \frac{1}{(kr)^2}\right] e^{-jkr}\hat{\theta}, \tag{27}$$

$$h_\phi = 0, \tag{28}$$

where $j = \sqrt{-1}$, k is the propagation constant, a is the coil radius, I_z is the coil current, r is the distance from the coil center, and N is the coil number of turns. Here, h_r, h_θ, and h_ϕ denote the magnetic fields in the r, θ, and ϕ direction in sperical coordinates, respectively.

There are various formulas to calculate the mutual inductance between coils, e.g., [127–129]. Most of these formulas are simplified based on the assumption that the receiving coil is in the near-field of the transmitting coil, which neglects the far-field. This is accurate for applications with closely separated transceivers. However, as the distance between a transmitter and a receiver increases, this mutual inductance model becomes inaccurate since the near-field components falloff fast and the receiver can obtain more power from the far-field radiation. We argue that the accurate way to obtain the mutual inductance is using $M = \phi/I_z$, where ϕ is the magnetic flux, that is

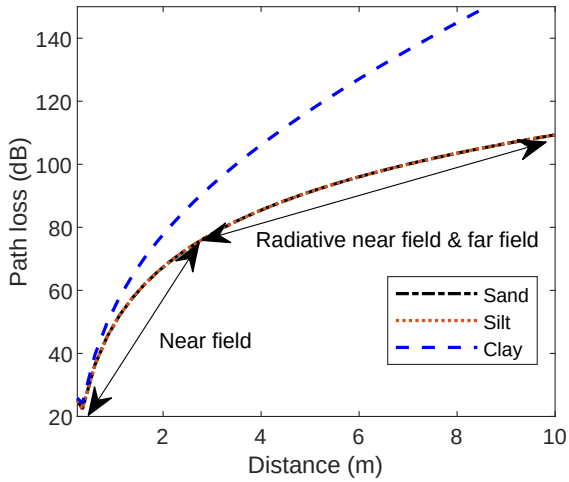

Fig. 10. Path loss for MI communication with 1 MHz carrier frequency. The path loss in the near field (the distance is approximately smaller than $\frac{\lambda}{2\pi}$) decreases much faster than that in the radiative near-field and the far-field.

generated by the transmitting coil with current I_z, through the receiving coil. Most of the existing works consider M as a positive real number. In fact, it can be real or complex and positive or negative, depending on coil orientations and the distance.

When $r \ll \lambda$, we consider the radiated fields are magnetoquasistatic (MQS). Under this condition, the near field components are dominant, and we can simplify the radiated field model by keeping the dominant terms with $1/r^3$. Also, we notice the mutual inductance M is a real number since the magnetic field does not propagate and there is no phase variation. The co-axial coils can provide the optimal received power since $h_r \approx 2h_\theta$. In this case, the induced EMF voltage in the receiving coil is

$$V_{emf} = -j\omega I_z M = -j\omega I_z \frac{\mu_0 N^2 \pi a^4}{2r^3} e^{-\frac{r}{\delta(f)}}, \tag{29}$$

where ω is the angular frequency, and $\delta(f)$ is the skin depth. The coil current is

$$|I_z| = \sqrt{\left|\frac{P_t}{Z_{in}}\right|} = \sqrt{\left|\frac{P_t}{Z_t + R_s + Z_{rt}}\right|}, \tag{30}$$

where $Z_t = R_{ac} + R_{rad} + j(\omega L - 1/(\omega C))$, Z_{in} is the transmitter input impedance, R_{ac} is the AC resistance, $Z_{rt} = \omega^2 M^2/(Z_r + Z_l)$ is the reflection impedance from the receiver, $Z_r = R_{ac} + R_{rad} + j(\omega L - 1/(\omega C))$ is the receiver's impedance, Z_l is the load impedance, R_{rad} is the radiation resistance, R_s is the source resistance, L is the self-inductance of the coil, and C the capacitance of the tuning capacitor. The received power can be written as

$$P_r = \Re(Z_l) \frac{|V_{emf}|^2}{|Z_r + Z_l + Z_{tr}|^2}, \tag{31}$$

where $Z_{tr} = \omega^2 M^2/(Z_t + R_s)$ is the reflected impedance from the transmitter to the receiver.

When $r \gg \lambda$, h_θ becomes the dominant term and it decreases as r, which is the same as electromagnetic waves in the free space. Thus, for the far field analysis, we can adopt existing wireless channel models at the corresponding frequency bands.

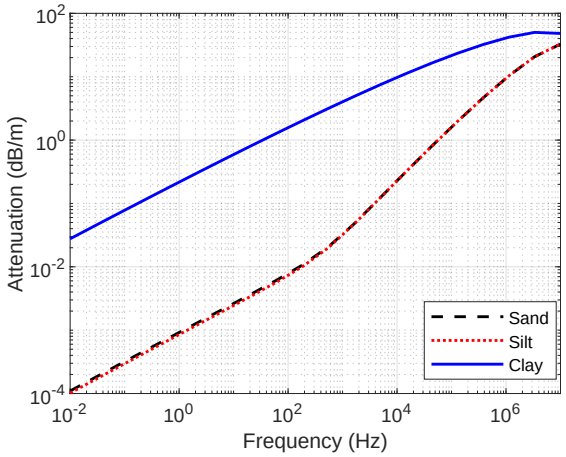

Fig. 11. Attenuation rate of MI communication through the soil. MI communication has different attenuation rate in the near field, the radiative near field and the far field. Here, we consider the communication range is $\frac{\lambda}{2\pi}$, which is almost the maximum distance that we can obtain by using near field MI communication.

Next, we numerically evaluate the path loss of MI communication. We consider three soil media, namely, sand, silt, and clay, and their dielectric parameters are given in [130]. In [130], permittivity is given as an average value for the three different media, but the conductivity is different. Here, we consider the water content is 0.3 cm^3/cm^3 and the relative permittivity is 16.899. The conductivity for sand, silt, and clay are 8.106×10^{-7} S/m, 6.912×10^{-7} S/m, and 9.094×10^{-2} S/m. The coil radius is 0.05 m and the number of turns is 10. The coil is made of copper with a wire diameter of 0.001 m. The underground soil medium is considered as homogeneous and infinitely large. In Fig. 10, the path loss by using 1 MHz carrier frequency is shown. Note that, when the distance is much smaller than the wavelength, the induced voltage in (29) becomes infinitely large, which is not true in reality. Here, we use the self-inductance as the upper bound of the mutual inductance. When the mutual inductance is larger than self-inductance due to the singularity, we use the self-inductance to approximate the mutual inductance. As shown in Fig. 10, the attenuation rates (path loss per meter) in the near field and the radiative near field and the far-field is different. Since the dielectric parameters for the sand and the silt are similar, the path losses are almost the same. The clay has higher conductivity and, thus, the path loss increases fast as the distance increases.

The attenuation rates with different frequencies are shown in Fig. 11. As we have learned from Fig. 10, the attenuation rates are different at different distances. Here, when we compare the attenuation rate, we scale the distance by using the associated wavelength at different frequencies. We use $\frac{\lambda}{2\pi}$ since it is approximately the maximum distance for the near field MI communication [100]. As shown in the figure, by using low frequency, one can achieve similar performance as the electromagnetic wave. However, it is easy to fabricate a low-profile magnetic coil at low-frequency bands, but it is not easy to design a small electric antenna at such bands due to the limitation of radiation resistance.

In the literature, MI communication channel models have been presented in various ways under different assumptions. Next, we summarize the widely used assumptions and the associated coil and channel models.

- *Strongly coupled, near field.* This condition indicates that the transmitter and the receiver are close, i.e., roughly the distance is shorter than $\lambda/(2\pi)$, and ωM is comparable to or larger than

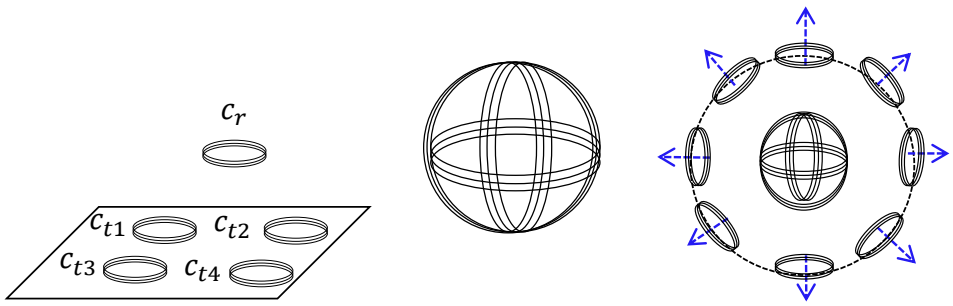

(a) Planar array. (b) Tri-axis coil. (c) Spherical array.

Fig. 12. Different types of magnetic coil arrays.

$R_{ac} + R_{rad}$. The developed model in (29), (30), and (31) can be used under this assumption. The models that are used in [99, 100, 112, 131, 132] fall into this category.

- *Loosely coupled, near field.* In this condition, the distance between the transmitter and the receiver is shorter than $\lambda/(2\pi)$, but due to the configuration of coils, e.g., the smaller number of turns or small coil size, ωM is much smaller than $R_{ac} + R_{rad}$ which can be safely neglected. As a result, we can ignore the Z_{rt} and Z_{tr} in (30) and (31). This simplifies the analysis of the MI communication channel since M is removed from the denominator of P_r. This assumption was used in [133, 134].
- *Loosely coupled, radiative near field.* In this condition, the communication range is longer than $\lambda/(2\pi)$, and the receiver leverages all the power, including reactive power and real power, to demodulate received signals. Thus, the MQS assumption is no longer valid, and we have to use (26) to derive the magnetic flux without any simplification. The models in [23, 107, 108]

Since MI communication is mainly used for short-range communication in extreme environments, its far filed applications are sparse.

5.1.3 Coil Orientation and Coil Array. The coil orientation has a tremendous impact on the MI channel, i.e., when coils are co-axially aligned, the received power is maximized, whereas when coils' orientation are perpendicular to each other, theoretically, the received power is zero no matter how close the transceivers are. To overcome this problem, coil arrays can be used to improve orientation diversity. There are mainly three categories of coil arrays depends on their geometry, namely, the planar array, the spherical array, and the tri-axis coils, as shown in Fig. 12.

Planar Array. The planar array was developed and used in [102–106]. As shown in Fig. 12, the planar array can transmit signals from a wide area rather than a single coil. As a result, the receiver, i.e., c_r, can obtain signals from multiple directions. With channel estimation, the transmitter can select the best transmit coil to further improve the communication efficiency.

Since the planar coil array occupies a small space in a portable wireless device, it has been widely adopted. There are two research lines in this direction. First, the coils are used as traditional antennas. The current in each coil is carefully designed to ensure that the magnetic fields at the receiver can be significantly enhanced. The signal processing algorithms are provided in [103, 104]. Second, some coils in an array are used to enhance or cancel the magnetic fields that are generated or received by other coils. In [102], the generated magnetic fields are enhanced to improve the received signal strength. In [105, 106], the coupling among coils is reduced to improve independent transmission to improve the channel capacity.

Tri-axis Coils. The use of tri-axis coils with three mutually perpendicular unidirectional coils efficiently addresses the problem of orientation loss [23, 107–114]. The underground environment is 3D and it is different from the terrestrial cellular wireless communication, where users are distributed on a 2D plane and omnidirectional communications can provide sufficient coverage. As a result, tri-axis coils are highly desirable since they can provide 3D coverage, i.e., they can transmit signals to and receive signals from any direction without blind areas. The tri-axis coil-based Multiple-Input-Multiple-Output (MIMO) model is presented in [108, 109]. Also, in [110], a novel modulation scheme is developed based on the tri-axis coil.

Spherical Array. The spherical coil array is motivated by the metamaterials, artificial materials that demonstrate abnormal dielectric properties, and designed to improve the radiated magnetic field intensity to extend the communication range in underground [116, 117]. As shown in Fig. 12(c), a tri-axis coil is placed in the center of a spherical array. Note that, the coils in the spherical array are uniformly distributed on a 3D spherical surface. Here, for better exposition, the coils that overlap with the tri-axis coil in the center are neglected. The resonance frequency of the coils in the spherical array is slightly higher than the operating frequency of the tri-axis coil. This is because these coils use smaller capacitance to ensure that the re-radiated magnetic fields have the same direction as the incident magnetic fields to improve the magnetic field intensity. The coils in the spherical array are passive and they do not have active inputs. The transmission signals are given for the tri-axis coil in the center. It was shown in [116] that without metallic loss in the spherical coil array, the enhanced magnetic field intensity can be 30 dB compared to that without the array. However, due to the metallic loss, in [117], the implemented spherical coil array has a gain of around 5 to 10 dB.

5.2 Modulation

Traditional modulation schemes can be used for MI communication without modification. The only difference is the low carrier frequency and narrow bandwidth. However, in the literature, there are some novel approaches to efficiently modulate signals for MI communication [110, 119, 120]. These modulation schemes are designed for MI communication, which will be reviewed in the following.

5.2.1 Direct Antenna Modulation. The Direct Antenna Modulation (DAM) is used to circumvent the problem of narrow bandwidth, which directly modulates signals on the antenna [120]. The magnetic coil is connected with a capacitor to achieve RLC resonance to improve its transmission efficiency. However, due to the resonance, the communication bandwidth is very narrow, which fundamentally limits the achievable communication data rate. The communication bandwidth B_w is limited by the coil quality factor Q_c

$$B_w \leq \frac{f_0}{Q_t}, \tag{32}$$

where f_0 is the carrier frequency. In MI communication, we demand a large Q_c improve the received signal strength. However, this significantly reduces the bandwidth.

The DAM proposed in [120] directly modulates signals on top of the carrier frequency. In Fig. 13, the equivalent circuit for a transmitter (left) and a receiver (right) is shown. The source has an input voltage of V_S and resistance R_S, and the receiver has a load resistance of R_L. The self-inductance, coil resistance, and tuning capacitance are L_1, R_{L1}, and C_1 for the transmitter and L_2, R_{L2}, and C_2 for the receiver, respectively. The Single Pole Double Throw (SPDT) switch is used to modulate 1 and 0.

For the traditional on-off modulation, a 1 is transmitted by using a nonzero V_S, and a 0 is transmitted by letting $V_S = 0$. Due to the narrow bandwidth, the switching frequency between 1

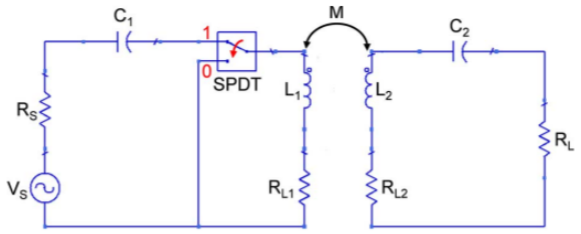

Fig. 13. Equivalent circuit model for MI communications using DAM modulation scheme. [120]

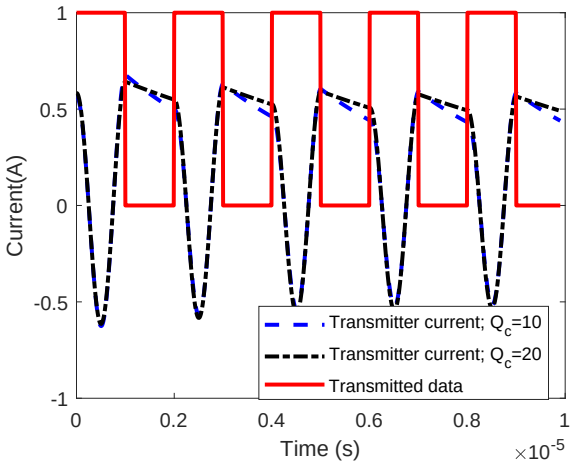

Fig. 14. Current of the transmitted coil with $Q_c = 10$ and $Q_c = 20$.

and 0 has to be small to discharge the capacitor. If the switching frequency is high, e.g., comparable to the carrier frequency, the difference between 1 and 0 is not obvious. For the DAM, when a 1 is transmitted, the SPDT switch to the capacitor to form a traditional RLC circuit. When a 0 is transmitted, the SPDT switch to the ground. In Fig. 14, we show an example of the transmission current for periodically sending the sequence of 10. As shown in the figure, we can clearly distinguish symbol 1 and symbol 0. Also, the larger the quality factor, the slower the discharge, i.e., the current for symbol 0 decreases slower. Since the switching frequency can be as high as the carrier frequency, the signal bandwidth is not limited by f_0/Q_c. This approach is especially useful for low carrier frequency applications where the signal bandwidth is extremely narrow.

5.2.2 Magnetic Vector Modulation. The Magnetic Vector Modulation (MVM) leverages the unique structure of tri-axis coils. Assume that the three unidirectional coils have currents I_x, I_y, and I_z, respectively. Thanks to the orientation diversity, receivers can detect the transmitting coil. For example, I_x can be set to 1 and I_y and I_z are 0. Then, the receiver detects the incident direction of the magnetic fields, upon which it can detect the current I_x. If I_x is positive, the transmitted symbol is 0. A complete symbol set is given in Table 4.

By using MVM, the data rate can be $\log(6)/\log(2) \approx 2.58$ times higher than simply using BPSK modulation. The proposed modulation for MI communication was tested in underground mines. The carrier frequency is around 2 kHz and the data rate is around 80 bps.

Table 4. Coil energizations for MVM. [110]

Symbol	I_x	I_y	I_z
0	+1	0	0
1	0	+1	0
2	0	0	+1
3	-1	0	0
4	0	-1	0
5	0	0	-1

5.3 Testbed

Besides theoretical works, there are several magnetic induction communication testbeds [104, 110–113, 117, 122–124, 135, 136]. These testbeds are mainly software-defined, i.e., the communication and networking protocols are programmable, and implemented using USRPs (Universal Software Radio Peripheral) [137] and microcontrollers with RF circuits. Although all of them are used for magnetic induction communication, their communication range, carrier frequency, and achievable data rate are very different, which depends on the specific applications and surrounding environments. Next, we introduce the key characteristics and implementation challenges of each testbed.

5.3.1 USRP-based Testbeds. USRP is a software-defined radio [138], which is developed by using FPGA. Since its hardware can be reconfigured, USRP can rapidly prototype wireless systems and test novel wireless communication and networking algorithms, which has been extensively adopted in wireless research. The LFTX and LFRX daughterboards can support DC to 30 MHz carrier frequency, which covers the whole operating frequency bands of magnetic induction communication. The daughterboards can be integrated on top of the motherboards in USRP N210 or N200. For the communication software implementation, the GNU radio [139], LabVIEW [140], and MATLAB/Simulink [141] provide well-developed packages and users can also customize their own algorithms. Since GNU radio is open source and users have more access to the core of the platform, it is more widely used. Also, LabVIEW has a very friendly user interface, which is easy to use. Most wireless communication researchers are familiar with MATLAB and their algorithms are developed in MATLAB. By using MATLAB to configure USRPs, one can easily prototype the developed algorithms.

In [113, 121], the magnetic induction communication testbeds are developed based on USRPs and GNU radio or MATLAB. The coils are tuned by using capacitors. In [113], a sinusoidal wave is transmitted and the received signals strength is measured to derive the path loss. The results show that using relay coils, the communication range is around 2 m in the underground. In [121], a more practical communication testbed was presented. The source generates binary data, which are modulated and transmitted.

5.3.2 Microcontroller-based Testbeds. Different from cellular communications or local area wireless networks, MI communication is a low-power low-cost technology to connect smart devices. Thanks to its low carrier frequency, it is possible to build a testbed using simple microcontrollers [104, 110–112, 122–124]. Due to its low-cost, testbeds design for magnetic induction communication along this direction is more popular than that using USRPs. These testbeds can be further divided into two categories, i.e., one is using standard communication transmitting and receiving chips [111, 112], and the other one is assembling wireless components such as power amplifiers, phase shifters, and gain controllers and build reconfigurable communication systems [104, 110, 122–124].

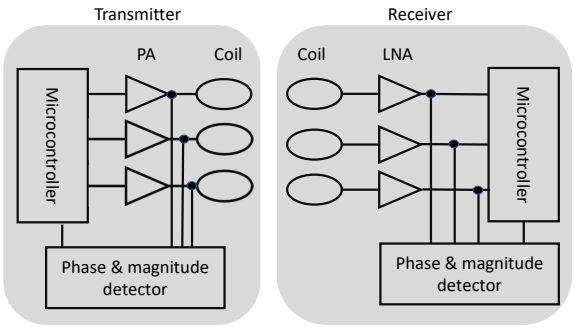

Fig. 15. Microcontroller-based magnetic induction MIMO communication.

Currently, wireless standards have employed magnetic induction communications, e.g., RFID at 125 kHz, RFID at 13.56 MHz, and NFC at 13.56 MHz. In [112], the testbed is designed by using the Freelinc Near Field Magnetic Induction radios, which has a current consumption of around 18 mA. The radio is used to control a tri-axis coil. The Philips LPC2148 ARM7TDMI microcontroller is used to program the radio. The communication range is around 10 m in an indoor laboratory environment. In [111], a testbed based on 125 kHz RFID chips was developed. The microcontroller is MSP430F5529, the transmitting chip is ATA5276, and the receiving chip is AS3933. Thanks to the low operating frequency, the communication range is around 40 m.

However, we cannot reconfigure standard chips to test novel wireless algorithms, and thus the above approach can prove the feasibility of magnetic communication, but it is not flexible enough to support research and development activities. In [104, 110, 122–124], various testbeds were developed by using customized components for applications in underground, underwater, and indoor. Testbeds using multiple coils were designed in [104, 124]. Although the application was wireless power transfer, it can be easily adopted for wireless communication since they share the fundamental magnetic induction principles. Besides microcontrollers and power amplifiers, these testbeds employed phase and magnitude detectors to coordinate the transmissions of multiple coils to create magnetic beams, upon which the power transfer efficiency and range can be improved. An illustration of the system architecture is shown in Fig. 15. This opens a door for magnetic induction communication to rapidly prototype MIMO (Multiple-Input-Multiple-Output) systems. Compared with USRP, which requires synchronization among devices, the microcontroller-based approach is low-cost.

Besides communication system design, some researchers also made great contributions to coil design and fabrication. Different from traditional antenna design, the coils are electrically small and have strong high-frequency resonances, which is hard to match and design. Readers are referred to [100, 117, 142, 143] for more details.

5.4 Applications

MI communication has been used to enable wireless connectivity for underground sensors. In [23, 144], MI communication is used to connect wireless devices in deep oil reservoirs. Traditional wireless technologies experience significant propagation loss due to the high conductivity of the mixed fluids in oil reservoirs. MI relay networks are designed to overcome this issue. A large number of coils are deployed in oil reservoirs to form a relay network to extend the communication range. As a result, the sensing data in deep oil reservoirs can be reported to above-ground control centers.

MI communication is also used to monitor underground pipelines [109, 145]. Traditional wireless sensor networks can only monitor near ground leakages, which can not report leakages in their early stages. The underground sensor networks using MI communication are deployed close to pipelines with around 1 m depth. Any minor leakage can be detected and reported immediately. Thanks to MI communication's high penetration efficiency, even in presence of oil leakage, it can efficiently transmit data to above ground. Also, the underground sensors for smart agriculture are envisioned to use MI communication to provide soil nutrition information to efficiently plan the use of fertilizers [146].

5.5 Open Research Problems

Although MI communication has been developed for around one decade, there are still a few challenges that need to be addressed. First, low-power MI communication is highly desired. The deployment of underground sensors requires significant efforts, and replacing sensors' battery is challenging, especially when the sensor number is large. Low-power MI communication can extend the lifetime of wireless underground sensors to alleviate the burden of battery replacement. The recently developed battery-free MI backscatter communication can be a viable solution [146]. Second, MI communication network design is complex. On one hand, the communication range is short, which allows multiple simultaneous communication links. On the other hand, it requires a large number of sensors to cover a wide area; the deployment is labor-intensive. To balance this trade-off, heterogeneous networks with long-range communication technologies may maintain high throughput while reducing the number of required sensors. Third, the integration of MI communication networks with existing wireless networks has not been visited yet. MI communication is used for underground applications, but the data have to be routed to existing wireless or wired networks. MI communication data rate is much lower than existing wireless solutions and the protocols different. The seamless integration is challenging.

6 OPTICAL UNDERGROUND COMMUNICATION

Optical signals do not pass through the soil and in general require line-of-sight, thus, optical medium cannot be used directly as a communication channel in such environment. However, optical communication has only been used for monitoring down-hole gas pipelines [147, 148]. The frequency response of the optical channel can be expressed as

$$H(f) = \int \sum_{i=1}^{N} P_i \delta\left(t - \tau\right) e^{-j2\pi f t} dt \tag{33}$$

where P_i and τ_i are the power and propagation delay of the i-th ray, and N is assumed to be the number of rays received at the receiver through multiple paths.

In [147] the light emitting diodes (LEDs) are used as a transmitter at the bottom of the down hole, whereas high sensitivity single photon detecting receivers are placed at the surface. The non-return-to-zero on-off keying (NRZ-OOK) is used for modulating the optical signals in this study. The lack of ambient light inside the gas pipelines enables high signal to noise ratio (SNR) at the receiver; thus, by exhausting only 8 dBm power, the transmitter can send the monitoring signal in a 4,000 metres long gas pipe with a datarate of 1 kbps. With more power of 32.1 dBm the transmitter can cover a linger range of 10,000 m while maintain a good quality communication.

In [148] the authors have used a pipeline of 22 m length and 1 m diameter with an interior made of carbon steel. An LED is used as a transmitter, while the receivers are kept 1 m apart through the pipeline. With these settings, the authors have achieved a distance coverage of 22 m with a 8-PAM (pulse amplitude modulation) with a bit-error-rate of 10^{-6}. The corresponding achieving distances

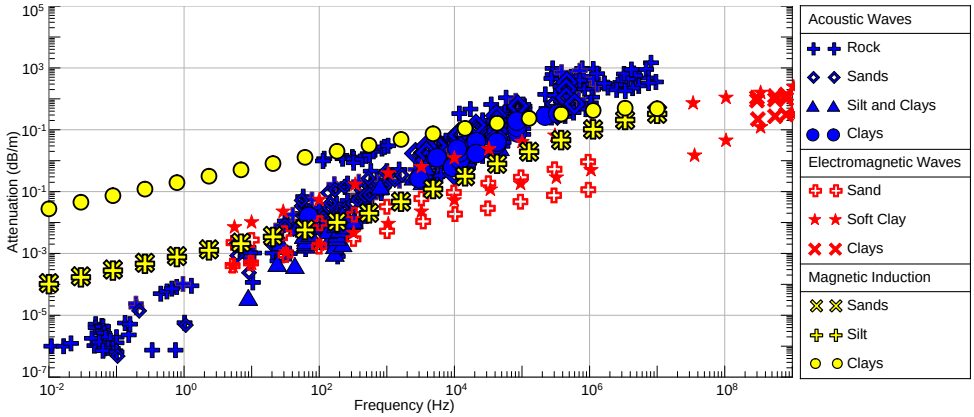

Fig. 16. Comparison of attenuation losses through soil among different wireless technologies, i.e., acoustic [60], electromagnetic [149, 150], and magnetic induction waves.

for 16-PAM, 32-PAM, 64-PAM, 128-PAM, 256-PAM and 512-PAM become 19.07 m, 13.64 m, 9.99 m, 7.32 m, 5.28 m and 3.82 m respectively. Thus, a single hop is sufficient to achieve a distance coverage of 22 m with a 8-PAM, whereas a single relay (r two hops) is sufficient for 16-PAM and 32-PAM. The higher order modulation sizes require more relays to achieve the BER target of 10^{-6}.

7 COMPARISON BETWEEN DIFFERENT TECHNOLOGIES

In this section we compare the various communication technologies for UWSNs along with their pros and cons. As optical communication is generally not used for UWSNs, we do not discuss it here. Fig. 16 shows a comparison of attenuation losses between different wireless communication technologies in case of underground environment.

The least cost and mature wireless communications technology is, of course RF (radio frequency) communications. The RF penetration in the ground decreases with increasing frequency, which makes lower frequencies more attractive; however, communication bandwidth suffers as result. The penetration distance depends on the electrical characteristics of the soil such as conductivity, which can vary greatly. In very moist or moist clay rich soils the penetration can be only a few centimeters. Furthermore, significant penetration requires too much communication energy. At the same time working in low frequencies requires long antennas, which are also not feasible in most of the applications. From Fig. 16 we can observe that even if RF propagation shows a low attenuation of 0.1 dB/m at 10 KHz, the RF transceivers require a quarter-wavelength antenna size of at least 3.75 Km to operate in this frequency.

Acoustic signals are less affected by the underground materials, and can achieve low attenuation at low frequencies. From Fig. 16 we can observe that RF exhibits lower attenuation at higher frequencies than acoustic, however, the attenuation values go up with increasing frequency. Fig. 16 also shows that acoustic communication can achieve low attenuation at low frequency band (i.e. below 100 Hz) with antennas smaller than 30 cm, and thus can reach few tens of meters in underground environments. However, the achievable data rate and bandwidth will be lower at this frequency range, which can be acceptable for low data rate WSN applications. The speed of sound is also much lesser than electromagnetic signals and thus suffers from low propagation delay, multipath effects and inter-symbol interference. All these severely limits the achievable datarate of

acoustic communication, typically less than 100 bps. Thus, the communication technique is suitable for low datarate, long-distance underground communications.

Table 5. Comparison of different underground communication technologies

Standard	RF	Acoustic	Magnetic
Frequency	2.4 GHz [39] 433-915 MHz [38, 51] 174 MHz [46] 3.1-10.6 GHz [42]	40-80 Hz [70, 80]	13.5 MHz [151] 131 [152] & 2–2.5 kHz [153]
Data rate	upto 124 Mbps [36]	2 bps - 2 kbps [70]	596 kbps [154]
Range	upto 12 m [36]	upto 50 m [70]	2-3 m (@13.5 MHz) [112] 10's of m (@131 kHz) [152] 30 m (@2.5 kHz) [153]
Peak current/power consumption	30 mA	9-30 W [70]	1.35 mA [154] 18 mA (FreeLinc) [151]

MI communication achieves both the goal of higher penetration in underground materials, as well as enjoys low propagation delays. MI devices can achieve datarates of ~608 kbps at 4-8 MHz within a communication distance of 2 meters [155], whereas longer range of 30 m through rock is achieved at a lower frequency of 2500 Hz with a low datarate upto ~100 bps [12]. However, the key challenge of MI communication is that the induced power drops off as the sixth power of the distance, thus making long range communication power hungry. The power transfer is proportional to the frequency, but because MI is a near field technology, the frequency for soil monitoring is limited to a few hundred KHz to few MHz range. The long-term operation of the MI based sensor network involves another crucial issue: a potential drift in the resonance frequency both due to changes in the soil characteristics and parameters (capacitance and inductance) of the MI circuit. The MI communication efficiency suffers rapidly as the mismatch between transmitter and receiver frequencies widens. Thus for long-term operation, it is essential to dynamically tune the circuit. This tuning requires a variable capacitor on the receiver and its closed loop control to track the transmitter frequency, which is extremely challenging to design. The comparison of different wireless underground communication technologies is summarized in Table ??.

7.1 Underground energy harvesting

A key challenge of underground communication is the energy sources of the underground sensors. It is difficult to replace batteries in an underground sensor networks when they die. Thus harvesting energy from different sources is an interesting research direction. Even if energy harvesting in sensor networks is extensively studied in terrestrial sensor networks, such techniques like solar or wind energy harvesting is not feasible in underground context. Even if the goal of this paper is to study the communication aspect, the techniques like RF, acoustic and MI can also be implemented for underground energy harvesting. An EM based underground energy harvesting in sub GHz frequency range is studied in [156, 157]. Wireless energy transfer with magnetically coupled inductive circuits, often referred to as wireless electricity (WiTricity) or Wireless Power Transfer (WPT) [158–160] has been studied for recharging the sensing nodes wirelessly. Although these techniques have been studied in air medium, as the magnetic signals can penetrate through underground, such techniques can also be applied for UWSNs. Various such techniques have been surveyed in [161].

Other than these above mentioned techniques, another source of energy harvesting is through vibration from some above-ground sources that create stress at the underground sensing points which can be converted to electricity by the buried piezo-electric harvesters. In the context of

agricultural UWSNs such vibration energy can be generated from several sources like tractors, seeders, sprayers etc. In [162] the authors have explored an analytical model of piezoelectric energy harvesting in a UWSN from an aboveground source. They have also done an experimental setup to measure the magnitude and frequency of such vibrations from the agricultural machines. Based on their outcomes, upto 17 mW can be achieved at a burial depth of 40 cm. Although vibration energy harvesting can be effective for sensors buried close to the ground, such effectiveness of such techniques goes down rapidly with the burial depths. Other harvesting techniques like energy harvesting from underground temperature change due to rain, snow can also be used, however, the effectiveness of such techniques require further investigations.

8 CONCLUSION

Owing to the rather complex channel characteristics of heterogeneous underground medium, i.e. soil, clay, sand, rocks, water etc., exploring robust communication is quite challenging due to numerous underground effects including soil attenuation, reflection, scattering, multipath effects etc. In this article, we have provided a comprehensive summary of various facets of underground propagation, and explored the strengths and limitations of different technologies in the context of different underground monitoring application areas.

To be specific, the article considers four different alternatives of underground propagation, namely radio communication, acoustics, magnetic and VLC. Among these technologies VLC shows limited promise because of cluttered underground environment, whereas the radio communication experiences high absorption, and quite affected by underground water level. Acoustic and magnetic communication appears as two promising technologies. The study also demonstrates different underground effects on these communication technologies through experimental observations. We hope that the structured treatment of the subject of underground, and the research summaries discussed in this paper will spur researchers to further examine the communication issues and limitations in the underground space.

REFERENCES

[1] "Soil," https://en.wikipedia.org/wiki/Soil.

[2] Y. Li, S. Wang, C. Jin, Y. Zhang, and T. Jiang, "A survey of underwater magnetic induction communications: Fundamental issues, recent advances, and challenges," *IEEE Communications Surveys Tutorials*, vol. 21, no. 3, pp. 2466–2487, thirdquarter 2019.

[3] M. Jouhari, K. Ibrahimi, H. Tembine, and J. Ben-Othman, "Underwater wireless sensor networks: A survey on enabling technologies, localization protocols, and internet of underwater things," *IEEE Access*, vol. 7, pp. 96 879–96 899, 2019.

[4] H.-J. Kim, H. Hirayama, S. Kim, K. J. Han, R. Zhang, and J.-W. Choi, "Review of near-field wireless power and communication for biomedical applications," *IEEE Access*, vol. 5, pp. 21 264–21 285, 2017.

[5] S. Yarkan, S. Guzelgoz, H. Arslan, and R. R. Murphy, "Underground mine communications: A survey," *IEEE Communications Surveys & Tutorials*, vol. 11, no. 3, pp. 125–142, 2009.

[6] A. K. Sharma, S. Yadav, S. N. Dandu, V. Kumar, J. Sengupta, S. B. Dhok, and S. Kumar, "Magnetic induction-based non-conventional media communications: A review," *IEEE Sensors Journal*, vol. 17, no. 4, pp. 926–940, 2016.

[7] S. Kisseleff, I. F. Akyildiz, and W. H. Gerstacker, "Survey on advances in magnetic induction-based wireless underground sensor networks," *IEEE Internet of Things Journal*, vol. 5, no. 6, pp. 4843–4856, 2018.

[8] N. Saeed, M.-S. Alouini, and T. Y. Al-Naffouri, "Towards the internet of underground things: A systematic survey," *IEEE Communications Surveys & Tutorials*, 2019.

[9] T. Ojha, S. Misra, and N. S. Raghuwanshi, "Wireless sensor networks for agriculture: The state-of-the-art in practice and future challenges," *Computers and Electronics in Agriculture*, vol. 118, pp. 66 – 84, 2015.

[10] R. J. N., T. B. C., and B. A. R., "Effect of drip irrigation and plastic mulch on yield, water use efficiency and benefit-cost ratio of pea cultivation," *Journal of the Indian Society of Soil Science*, vol. 46, no. 4, pp. 562–567, 1998.

[11] S. von Westarp, S. Chieng, and H. Schreier, "A comparison between low-cost drip irrigation, conventional drip irrigation, and hand watering in nepal," *Agricultural Water Management*, vol. 64, no. 2, pp. 143–160, 2004.

[12] A. Markham and N. Trigoni, "Magneto-inductive networked rescue system (MINERS): taking sensor networks underground," in *IPSN*, 2012, pp. 317–328.

[13] "Underground coal mining disasters and fatalities — united states, 1900–2006," https://www.cdc.gov/mmwr/preview/mmwrhtml/mm5751a3.htm, 2009.
[14] "2010 chilean mine rescue fast facts," https://www.cnn.com/2013/07/13/world/americas/chilean-mine-rescue/index.html, 2020.
[15] M. V. Ramesh, "Design, development, and deployment of a wireless sensor network for detection of landslides," *Ad Hoc Networks*, vol. 13, pp. 2–18, 2014.
[16] M. E. Cambron, C. Brode, P. Butler, and G. Olszewkski, "Poacher detection at fence crossing," in *IEEE SoutheastCon*, 2015.
[17] "Iucn red list of threatened species," 2008.
[18] J. Kamminga, E. D. Ayele, N. Meratnia, and P. Havinga, "Poaching detection technologies—a survey," *Sensors*, vol. 18, p. 1474, 2018.
[19] M. J. Chase, S. Schlossberg, C. R. Griffin, P. Bouché, S. W. Djene, P. W. Elkan, S. M. Ferreira, F. Grossman, E. M. Kohi, K. Landen, P. Omondi, A. Peltier, S. A. J. Selier, and R. P. Sutcliffe, "Continent-wide survey reveals massive decline in african savannah elephants," *PeerJ*, vol. 4, 2016.
[20] A. Markham, N. Trigoni, S. A. Ellwood, and D. W. Macdonald, "Revealing the hidden lives of underground animals using magneto-inductive tracking," in *ACM SenSys*, J. Beutel, D. Ganesan, and J. A. Stankovic, Eds., 2010, pp. 281–294.
[21] M. Li and Y. Liu, "Underground coal mine monitoring with wireless sensor networks," *ACM Trans. Sens. Networks*, vol. 5, no. 2, pp. 10:1–10:29, 2009.
[22] M. A. Akkaş, R. Sokullu, and A. Balcı, "Wireless sensor networks in oil pipeline systems using electromagnetic waves," in *ELECO*, 2015, pp. 143–147.
[23] H. Guo and Z. Sun, "Channel and energy modeling for self-contained wireless sensor networks in oil reservoirs," *IEEE Transactions on Wireless Communications*, vol. 13, no. 4, pp. 2258–2269, 2014.
[24] I. Zaman and A. Förster, "Challenges and opportunities of wireless underground sensor networks," https://www.researchgate.net/publication/327844401, 2018.
[25] L. Li, M. C. Vuran, and I. F. Akyildiz, "Characteristics of underground channel for wireless underground sensor networks," in *Mediterranean Ad Hoc Networking WorkShop*, 2007, pp. 92–99.
[26] H. R. Bogena, J. A. Huisman, H. Meier, U. Rosenbaum, and A. Weuthen, "Hybrid wireless underground sensor networks: Quantification of signal attenuation in soil," *Vadose Zone Journal*, vol. 8, no. 3, pp. 755–761, 2009.
[27] Nchimunya Chaamwe, Wenyu Liu, and Hongbo Jiang, "Wave propagation communication models for wireless underground sensor networks," in *IEEE International Conference on Communication Technology*, 2010, pp. 9–12.
[28] N. R. Peplinski, F. T. Ulaby, and M. C. Dobson, "Dielectric properties of soils in the 0.3–1.3-ghz range," *IEEE Transactions on Geoscience and Remote Sensing*, vol. 33, no. 3.
[29] M. C. Vuran and I. F. Akyildiz, "Channel model and analysis for wireless underground sensor networks in soil medium," *Phys. Commun.*, vol. 3, no. 4, pp. 245–254, 2010.
[30] M. Vuran and A. Silva, *Communication Through Soil in Wireless Underground Sensor Networks – Theory and Practice*, 01 2009, pp. 309–347.
[31] J. Rhoades, P. Raats, and R. Prather, "Effects of liquid-phase electrical conductivity, water content, and surface conductivity on bulk soil electrical conductivity1," *Soil Science Society of America Journal*, vol. 40, pp. 651–655, 01 1976.
[32] S. Yoon, E. Ghazanfari, L. Cheng, S. Pamukcu, and M. T. Suleiman, "Subsurface event detection and classification using wireless signal networks," *Sensors*, vol. 12, no. 11, pp. 14 862–14 886, 2012.
[33] S. Yoon, L. Cheng, E. Ghazanfari, Z. Wang, X. Zhang, S. Pamukcu, and M. T. Suleiman, "Subsurface monitoring using low frequency wireless signal networks," in *IEEE PerCom Workshop*, 2012, pp. 443–446.
[34] M. A. Akkas, I. F. Akyildiz, and R. Sokullu, "Terahertz channel modeling of underground sensor networks in oil reservoirs," in *IEEE GLOBECOM*, 2012, pp. 543–548.
[35] S. Suherman, A. Rambe, W. Agustiar, and Tanjung, "Underground radio propagation on frequency band 97 mhz-130 mhz," *International Journal of Engineering and Technology*, vol. 7, pp. 722–726, 2018.
[36] A. Salam and M. C. Vuran, "Impacts of soil type and moisture on the capacity of multi-carrier modulation in internet of underground things," in *ICCCN*, 2016, pp. 1–9.
[37] ——, "Wireless underground channel diversity reception with multiple antennas for internet of underground things," in *IEEE ICC*, 2017, pp. 1–7.
[38] A. R. Silva and M. C. Vuran, "Development of a testbed for wireless underground sensor networks," *EURASIP J. Wireless Comm. and Networking*, no. 620307, 2010.
[39] S. Yoon, L. Cheng, E. Ghazanfari, S. Pamukcu, and M. T. Suleiman, "A radio propagation model for wireless underground sensor networks," in *IEEE GLOBECOM*, 2011, pp. 1–5.
[40] R. Goyal, R. Kennedy, B. Kelsey, M. Whelan, and K. Janoyan, *Underground Wireless Sensor Networks Using 2nd Generation RF Transceivers*, pp. 2619–2629. [Online]. Available: https://ascelibrary.org/doi/abs/10.1061/9780784413272.253

[41] X. Yu, Z. Zhang, and W. Han, "Evaluation of communication in wireless underground sensor networks," *IOP Conference Series: Earth and Environmental Science*, vol. 69, p. 012083, 2017.
[42] H. Zemmour, G. Baudoin, and A. Diet, "Soil effects on the underground-to-aboveground communication link in ultrawideband wireless underground sensor networks," *IEEE Antennas and Wireless Propagation Letters*, vol. 16, pp. 218–221, 2017.
[43] D. Du, H. Zhang, J. Yang, and P. Yang, "Propagation characteristics of the underground-to-aboveground communication link about 2.4ghz and 433mhz radio wave: An empirical study in the pine forest of guizhou province," in *IEEE ICCC*, 2017, pp. 1041–1045.
[44] B. Silva, R. M. Fisher, A. Kumar, and G. P. Hancke, "Experimental link quality characterization of wireless sensor networks for underground monitoring," *IEEE Transactions on Industrial Informatics*, vol. 11, no. 5, pp. 1099–1110, 2015.
[45] X. Zhang, A. Andreyev, C. Zumpf, M. C. Negri, S. Guha, and M. Ghosh, "Thoreau: A subterranean wireless sensing network for agriculture and the environment," in *IEEE INFOCOM Workshops*, 2017, pp. 78–84.
[46] R. Cardell-Oliver, C. Hübner, M. Leopold, and J. Beringer, "Dataset: Lora underground farm sensor network," in *DATA@SenSys*, 2019, pp. 26–28.
[47] A. Salam, M. C. Vuran, and S. Irmak, "Di-sense: In situ real-time permittivity estimation and soil moisture sensing using wireless underground communications," *Comput. Networks*, vol. 151, pp. 31–41, 2019.
[48] J. Tiusanen, "Wireless soil scout prototype radio signal reception compared to the attenuation model," *Precision Agriculture*, vol. 10, no. 5, pp. 372–381, 2009.
[49] "Mote-kit mica2," http://www.cmt-gmbh.de/Produkte/WirelessSensorNetworks/Datenblaetter/MOTE-KIT_MICA2_Datasheet.pdf.
[50] "Micaz," http://www.openautomation.net/uploadsproductos/micaz_datasheet.pdf.
[51] "Synapserf300 series engines," https://media.digikey.com/pdf/Data%20Sheets/Synapse%20PDFs/RF300_Br.pdf.
[52] C. Meehan, S. Kumar, M. Pando, J. Coe, O. Baltaji, S. Yang, Y. Hashash, and A. Singer, "Through-soil wireless communication system for embedded geotechnical instrumentation," in *Geotechnical Special Publication*, ser. Geotechnical Special Publication, M. Pando, J. Coe, C. Meehan, and S. Kumar, Eds., no. GSP 313. American Society of Civil Engineers (ASCE), 2019, pp. 200–208.
[53] M. Stojanovic and J. C. Preisig, "Underwater acoustic communication channels: Propagation models and statistical characterization," *IEEE Communications Magazine*, vol. 47, no. 1, pp. 84–89, 2009.
[54] M. Stojanovic, "Underwater acoustic communications," in *IEEE Electro International*, 1995, pp. 435–440.
[55] G. Lee, J. Lee, T. Kang, K. Kim, and W. Kim, "Experimental results of long range underwater communication based on chirp-fh signals," in *ICUFN*, 2019, pp. 39–41.
[56] G. A. Shah, "A survey on medium access control in underwater acoustic sensor networks," in *International Conference on Advanced Information Networking and Applications Workshops*, 2009, pp. 1178–1183.
[57] T. Riedl and A. Singer, "Towards a video-capable wireless underwater modem: Doppler tolerant broadband acoustic communication," in *2014 Underwater Communications and Networking (UComms)*. IEEE, 2014, pp. 1–5.
[58] S. L. Kramer *et al.*, *Geotechnical earthquake engineering*. Pearson Education India, 1996.
[59] B. A. Brunson, "A comparison between biot model predictions and shear wave attenuation measurements in unconsolidated laboratory sediments," *The Journal of the Acoustical Society of America*, vol. 74, no. S1, pp. S59–S59, 1983.
[60] A. C. Kibblewhite, "Attenuation of sound in marine sediments: A review with emphasis on new low-frequency data," *The Journal of the Acoustical Society of America*, vol. 86, no. 2, pp. 716–738, 1989.
[61] M. Vucetic and R. Dobry, "Effect of soil plasticity on cyclic response," *Journal of geotechnical engineering*, vol. 117, no. 1, pp. 89–107, 1991.
[62] E. Hamilton, "Acoustic properties of sediments," *Acoustics and ocean bottom*, pp. 3–58, 1987.
[63] D.-S. Kim and J.-S. Lee, "Propagation and attenuation characteristics of various ground vibrations," *Soil dynamics and Earthquake engineering*, vol. 19, no. 2, pp. 115–126, 2000.
[64] W. Nyborg, I. Rudnick, and H. Schilling, "Experiments on acoustic absorption in sand and soil," *The Journal of the Acoustical Society of America*, vol. 22, no. 4, pp. 422–425, 1950.
[65] W. D. O'Brien Jr, R. G. Darmondy, and D. C. Munson Jr, "Acoustic characterization of soil," ILLINOIS UNIV AT URBANA-CAMPAIGN BECKMAN INST FOR ADVANCED SCIENCES AND ..., Tech. Rep., 1996.
[66] M. L. Oelze, W. D. O'Brien, and R. G. Darmody, "Measurement of attenuation and speed of sound in soils," *Soil Science Society of America Journal*, vol. 66, no. 3, pp. 788–796, 2002.
[67] B. O. Hardin and V. P. Drnevich, "Shear modulus and damping in soils: design equations and curves," *Journal of Soil Mechanics & Foundations Div*, vol. 98, no. sm7, 1972.
[68] E. L. Hamilton, "Prediction of deep-sea sediment properties: state-of-the-art," in *Deep-Sea Sediments*. Springer, 1974, pp. 1–43.

[69] ——, "Geoacoustic modeling of the sea floor," *The Journal of the Acoustical Society of America*, vol. 68, no. 5, pp. 1313–1340, 1980.
[70] S. Yang, O. Baltaji, A. C. Singer, and Y. M. Hashash, "Development of an underground through-soil wireless acoustic communication system," *IEEE Wireless Communications*, vol. 27, no. 1, pp. 154–161, 2019.
[71] M. Biot, "Theory of elastic waves in a fluid-saturated porous solid. 1. low frequency range," *J. Acoust. Soc. Am.*, vol. 28, pp. 168–178, 1956.
[72] M. A. Biot, "Theory of propagation of elastic waves in a fluid-saturated porous solid. ii. higher frequency range," *The Journal of the acoustical Society of america*, vol. 28, no. 2, pp. 179–191, 1956.
[73] R. D. Stoll and G. M. Bryan, "Wave attenuation in saturated sediments," *The Journal of the Acoustical Society of America*, vol. 47, no. 5B, pp. 1440–1447, 1970.
[74] J. M. Hovem and G. D. Ingram, "Viscous attenuation of sound in saturated sand," *The Journal of the Acoustical Society of America*, vol. 66, no. 6, pp. 1807–1812, 1979.
[75] W. Nyborg, I. Rudnick, and H. Schilling, "Experiments on acoustic absorption in sand and soil," *The Journal of the Acoustical Society of America*, vol. 22, no. 4, pp. 422–425, 1950.
[76] J. W. Spencer Jr, "Bulk and shear attenuation in berea sandstone: The effects of pore fluids," *Journal of Geophysical Research: Solid Earth*, vol. 84, no. B13, pp. 7521–7523, 1979.
[77] K. W. Winkler and A. Nur, "Seismic attenuation: Effects of pore fluids and frictional-sliding," *Geophysics*, vol. 47, no. 1, pp. 1–15, 1982.
[78] J. W. Spencer Jr, "Stress relaxations at low frequencies in fluid-saturated rocks: Attenuation and modulus dispersion," *Journal of Geophysical Research: Solid Earth*, vol. 86, no. B3, pp. 1803–1812, 1981.
[79] P. M. Shankar, "A general statistical model for ultrasonic backscattering from tissues," *IEEE transactions on ultrasonics, ferroelectrics, and frequency control*, vol. 47, no. 3, pp. 727–736, 2000.
[80] K. Ikrath and W. Schneider, "Communications via seismic waves employing 80-hz resonant seismic transducers," *IEEE Transactions on Communication Technology*, vol. 16, no. 3, pp. 439–444, 1968.
[81] T. D. Brumleve, M. G. Hicks, and M. O. Jones, "System for remote control of underground device," Oct. 21 1975, uS Patent 3,914,732.
[82] J. L. Harmon and W. T. Bell, "Downhole process control method utilizing seismic communication," Jun. 24 2003, uS Patent 6,584,406.
[83] O. Baltaji, S. Yang, Y. M. Hashash, and A. Singer, "Through-soil wireless communication system for embedded geotechnical instrumentation," in *Geo-Congress 2019: Soil Erosion, Underground Engineering, and Risk Assessment*. American Society of Civil Engineers Reston, VA, 2019, pp. 200–208.
[84] M. A. Gutierrez-Estevez, U. Krüger, K. A. Krueger, K. Manolakis, V. Jungnickel, K. Jaksch, K. Krüger, S. Mikulla, R. Giese, M. Sohmer, and M. Reich, "Acoustic broadband communications over deep drill strings using adaptive OFDM," in *IEEE WCNC*, 2013, pp. 4089–4094.
[85] J. M. Neff and P. L. Camwell, "Field test results of an acoustic telemetry mwd system," in *IADC/SPE Drilling Conference*, 2007.
[86] A. Farraj, S. Miller, and K. Qaraqe, "Channel characterization for acoustic downhole communication systems," in *SPE Annual Technical Conference and Exhibition*, 2012.
[87] A. Farraj, "Acoustical communications for wireless downhole telemetry system," Ph.D. dissertation, Texas AM University, 2012.
[88] W. Gardner, R. Hyden, E. Linyaev, L. Gao, C. Robbins, and J. Moore, "Acoustic telemetry delivers more real-time downhole data in underbalanced drilling operations," in *IADC/SPE Drilling Conference*, 2006.
[89] M. A. Gutierrez-Estevez, U. Krüger, K. A. Krueger, K. Manolakis, and V. Jungnickel, "Acoustic channel model for adaptive downhole communication over deep drill strings," in *IEEE ICASSP*, 2013, pp. 4883–4887.
[90] S. Sinanovic, D. H. Johnson, V. V. Shah, and W. R. Gardner, in *IEEE ICASSP*, 2004.
[91] D. Ma, Y. Shi, W. Zhang, and G. Liu, "Design of acoustic transmission along drill strings for logging while drilling data based on adaptive nc-ofdm," *AEU - International Journal of Electronics and Communications*, vol. 83, 09 2017.
[92] Z. Wei, S. Yibing, and L. Yanjun, "Design of acoustic wireless remote transmission system for logging-while-drilling data," in *IEEE ICEMI*, 2013, pp. 53–57.
[93] T. J. Ahmad, M. Noui-Mehidi, and M. Arsalan, "Performance analysis of downhole acoustic communication in multiphase flow," in *IEEE IECON*, 2014, pp. 3909–3913.
[94] K. Pelekanakis, M. A. Chitre, L. S. Kumar, and Y. L. Guan, "Performance of channel coding and equalization for acoustic telemetry along drill strings," in *IEEE International Conference on Communication Systems, ICCS 2014, Macau, China, November 19-21, 2014*, 2014, pp. 610–614.
[95] A. Alenezi and A. Abdi, "A comparative study of multichannel and single channel accelerometer sensors for communication in oil wells," in *2017 International Conference on Communication and Signal Processing (ICCSP)*, 2017, pp. 0153–0156.

[96] I. Bogie, "Conduction and magnetic signalling in the sea a background review," *Radio and Electronic Engineer*, vol. 42, no. 10, pp. 447–452, 1972.
[97] A. Pal and K. Kant, "NFMI: connectivity for short-range iot applications," *Computer*, vol. 52, no. 2, pp. 63–67, 2019.
[98] ——, "NFMI: near field magnetic induction based communication," *Elsevier Computer Networks*, 2020.
[99] Z. Sun and I. F. Akyildiz, "Magnetic induction communications for wireless underground sensor networks," *IEEE Transactions on Antennas and Propagation*, vol. 58, no. 7, pp. 2426–2435, 2010.
[100] Y. Morag, N. Tal, Y. Leviatan, and Y. Levron, "Channel capacity of magnetic communication in a general medium incorporating full-wave analysis and high-frequency effects," *IEEE Transactions on Antennas and Propagation*, vol. 67, no. 6, pp. 4104–4118, 2019.
[101] D. O. LeVan, "Novel communication channel model for signal propagation and loss through layered earth," *IEEE Transactions on Geoscience and Remote Sensing*, vol. 58, no. 8, pp. 5393–5399, 2020.
[102] H. Guo and Z. Sun, "Increasing the capacity of magnetic induction communication using mimo coil-array," in *Global Communications Conference (GLOBECOM), 2016 IEEE*. IEEE, 2016, pp. 1–6.
[103] G. Yang, M. R. V. Moghadam, and R. Zhang, "Magnetic mimo signal processing and optimization for wireless power transfer," *IEEE Transactions on Signal Processing*, vol. 65, no. 11, pp. 2860–2874, 2017.
[104] J. Jadidian and D. Katabi, "Magnetic mimo: How to charge your phone in your pocket," in *Proceedings of the 20th annual international conference on Mobile computing and networking*. ACM, 2014, pp. 495–506.
[105] H.-J. Kim, K. Kim, S. Han, D.-W. Seo, and J.-W. Choi, "Nearly non-coupling coil array allowing many independent channels for magnetic communication," *IEEE Access*, vol. 6, pp. 34 190–34 197, 2018.
[106] H.-J. Kim, J. Park, K.-S. Oh, J. P. Choi, J. E. Jang, and J.-W. Choi, "Near-field magnetic induction mimo communication using heterogeneous multipole loop antenna array for higher data rate transmission," *IEEE Transactions on Antennas and Propagation*, vol. 64, no. 5, pp. 1952–1962, 2016.
[107] H. Guo, Z. Sun, and P. Wang, "Channel modeling of mi underwater communication using tri-directional coil antenna," in *Global Communications Conference (GLOBECOM), 2015 IEEE*. IEEE, 2015, pp. 1–6.
[108] ——, "Multiple frequency band channel modeling and analysis for magnetic induction communication in practical underwater environments," *IEEE Transactions on Vehicular Technology*, vol. 66, no. 8, pp. 6619–6632, 2017.
[109] H. Guo and K. D. Song, "Reliable through-metal wireless communication using magnetic induction," *IEEE Access*, vol. 7, pp. 115 428–115 439, 2019.
[110] A. Markham and N. Trigoni, "Magneto-inductive networked rescue system (miners): taking sensor networks underground," in *Proceedings of the 11th international conference on Information Processing in Sensor Networks*. ACM, 2012, pp. 317–328.
[111] N. Ahmed, A. Radchenko, D. Pommerenke, and Y. R. Zheng, "Design and evaluation of low-cost and energy-efficient magneto-inductive sensor nodes for wireless sensor networks," *IEEE Systems Journal*, vol. 13, no. 2, pp. 1135–1144, 2018.
[112] R. K. Gulati, A. Pal, and K. Kant, "Experimental evaluation of a near-field magnetic induction based communication system," in *IEEE Wireless Communications and Networking Conference (WCNC)*. IEEE, 2019, pp. 1–6.
[113] X. Tan, Z. Sun, and I. F. Akyildiz, "Wireless underground sensor networks: Mi-based communication systems for underground applications." *IEEE Antennas and Propagation Magazine*, vol. 57, no. 4, pp. 74–87, 2015.
[114] I. F. Akyildiz, P. Wang, and Z. Sun, "Realizing underwater communication through magnetic induction," *IEEE Communications Magazine*, vol. 53, no. 11, pp. 42–48, 2015.
[115] Z. Zhang, E. Liu, X. Qu, R. Wang, H. Ma, and Z. Sun, "Connectivity of magnetic induction-based ad hoc networks," *IEEE Transactions on Wireless Communications*, vol. 16, no. 7, pp. 4181–4191, 2017.
[116] H. Guo, Z. Sun, J. Sun, and N. M. Litchinitser, "M^2I: Channel Modeling for Metamaterial-Enhanced Magnetic Induction Communications," *IEEE Transactions on Antennas and Propagation*, vol. 63, no. 11, pp. 5072–5087, 2015.
[117] H. Guo, Z. Sun, and C. Zhou, "Practical design and implementation of metamaterial-enhanced magnetic induction communication," *IEEE Access*, vol. 5, pp. 17 213–17 229, 2017.
[118] Z. Li and Z. Sun, "Antenna system optimization for active metamaterial-enhanced magnetic induction communications," in *2019 13th European Conference on Antennas and Propagation (EuCAP)*. IEEE, 2019, pp. 1–5.
[119] S. Kisseleff, I. F. Akyildiz, and W. H. Gerstacker, "Digital signal transmission in magnetic induction based wireless underground sensor networks," *IEEE Transactions on Communications*, vol. 63, no. 6, pp. 2300–2311, 2015.
[120] U. Azad and Y. E. Wang, "Direct antenna modulation (dam) for enhanced capacity performance of near-field communication (nfc) link," *IEEE Transactions on Circuits and Systems I: Regular Papers*, vol. 61, no. 3, pp. 902–910, 2014.
[121] D. Wei, L. Yan, C. Huang, J. Wang, J. Chen, M. Pan, and Y. Fang, "Dynamic magnetic induction wireless communications for autonomous underwater vehicle assisted underwater iot," *IEEE Internet of Things Journal*, 2020.
[122] A. Markham, N. Trigoni, S. A. Ellwood, and D. W. Macdonald, "Revealing the hidden lives of underground animals using magneto-inductive tracking," in *Proceedings of the 8th ACM Conference on Embedded Networked Sensor Systems*. ACM, 2010, pp. 281–294.

[123] D. Wei, L. Yan, X. Li, J. Wang, J. Chen, M. Pan, and Y. R. Zheng, "Ferrite assisted geometry-conformal magnetic induction antenna and subsea communications for auvs," in *2018 IEEE Global Communications Conference (GLOBECOM)*. IEEE, 2018, pp. 1–6.
[124] G. Cao, H. Zhou, H. Zhang, J. Xu, P. Yang, and X.-Y. Li, "Requirement-driven magnetic beamforming for mimo wireless power transfer optimization," in *2018 15th Annual IEEE International Conference on Sensing, Communication, and Networking (SECON)*. IEEE, 2018, pp. 1–9.
[125] H. Guo, "Performance analysis of near-field magnetic induction communication in extreme environments," *Progress In Electromagnetics Research Letters*, vol. 90, pp. 77–83, 2020.
[126] C. Balanis, *Antenna Theory: Analysis and Design*. Wiley, 2015.
[127] W. G. Hurley and M. C. Duffy, "Calculation of self and mutual impedances in planar magnetic structures," *IEEE Transactions on Magnetics*, vol. 31, no. 4, pp. 2416–2422, 1995.
[128] E. B. Rosa and F. W. Grover, *Formulas and tables for the calculation of mutual and self-inductance*. US Government Printing Office, 1948, no. 169.
[129] S. Babic, F. Sirois, C. Akyel, and C. Girardi, "Mutual inductance calculation between circular filaments arbitrarily positioned in space: Alternative to grover's formula," *IEEE transactions on magnetics*, vol. 46, no. 9, pp. 3591–3600, 2010.
[130] R. Porretta and F. Bianchi, "Profiles of relative permittivity and electrical conductivity from unsaturated soil water content models," *Annals of Geophysics*, vol. 59, no. 3, p. 0320, 2016.
[131] S. Kisseleff, W. Gerstacker, R. Schober, Z. Sun, and I. F. Akyildiz, "Channel capacity of magnetic induction based wireless underground sensor networks under practical constraints," in *Wireless Communications and Networking Conference (WCNC), 2013 IEEE*. IEEE, 2013, pp. 2603–2608.
[132] A. Pal and K. Kant, "Magnetic induction based sensing and localization for fresh food logistics," in *2017 IEEE 42nd Conference on Local Computer Networks (LCN)*. IEEE, 2017, pp. 383–391.
[133] S.-C. Lin, A. A. Alshehri, P. Wang, and I. F. Akyildiz, "Magnetic induction-based localization in randomly deployed wireless underground sensor networks," *IEEE Internet of Things Journal*, vol. 4, no. 5, pp. 1454–1465, 2017.
[134] Z. Sun and I. F. Akyildiz, "On capacity of magnetic induction-based wireless underground sensor networks," in *2012 Proceedings IEEE INFOCOM*. IEEE, 2012, pp. 370–378.
[135] H. Guo and Z. Sun, "Demo abstract: Prototyping M^2I communication system for underground and underwater networks," in *2017 IEEE Conference on Computer Communications Workshops (INFOCOM WKSHPS)*. IEEE, 2017, pp. 962–963.
[136] H. Guo, "Through-metal wireless communications with magnetic induction," in *2018 6th IEEE International Conference on Wireless for Space and Extreme Environments (WiSEE)*. IEEE, 2018, pp. 42–47.
[137] USRP. www.ettus.com/products/.
[138] M. Dillinger, K. Madani, and N. Alonistioti, *Software defined radio: Architectures, systems and functions*. John Wiley & Sons, 2005.
[139] GNU Radio. www.gnuradio.org/.
[140] LabVIEW. www.ni.com/en-us/shop/labview.html.
[141] MATLAB. www.mathworks.com/products/matlab.html.
[142] N. Tal, Y. Morag, L. Shatz, and Y. Levron, "Design optimization of transmitting antennas for weakly coupled magnetic induction communication systems," *PloS one*, vol. 12, no. 2, p. e0171982, 2017.
[143] N. Tal, Y. Morag, and Y. Levron, "Magnetic induction antenna arrays for mimo and multiple-frequency communication systems," *Progress In Electromagnetics Research*, vol. 75, pp. 155–167, 2017.
[144] L. Yan, D. Wei, M. Pan, and J. Chen, "Downhole wireless communication using magnetic induction technique," in *2018 United States National Committee of URSI National Radio Science Meeting (USNC-URSI NRSM)*. IEEE, 2018, pp. 1–2.
[145] Z. Sun, P. Wang, M. C. Vuran, M. A. Al-Rodhaan, A. M. Al-Dhelaan, and I. F. Akyildiz, "Mise-pipe: Magnetic induction-based wireless sensor networks for underground pipeline monitoring," *Ad Hoc Networks*, vol. 9, no. 3, pp. 218–227, 2011.
[146] H. Guo and Z. Sun, "Inter-media backscatter communications with magnetic induction," in *2019 IEEE International Conference on Communications (ICC)*. IEEE, 2019, pp. 1–6.
[147] Y. Li, S. Videv, M. Abdallah, K. Qaraqe, M. Uysal, and H. Haas, "Single photon avalanche diode (spad) vlc system and application to downhole monitoring," in *IEEE Global Communications Conference*, 2014, pp. 2108–2113.
[148] F. Miramirkhani, M. Uysal, O. Narmanlioglu, M. Abdallah, and K. Qaraqe, "Visible light channel modeling for gas pipelines," *IEEE Photonics Journal*, vol. 10, no. 2, pp. 1–10, 2018.
[149] K. Klein and J. C. Santamarina, "Methods for broad-band dielectric permittivity measurements (soil-water mixtures, 5 hz to 1.3 ghz)," *Geotechnical Testing Journal*, vol. 20, no. 2, pp. 168–178, 1997.
[150] A. R. Silva and M. C. Vuran, "Communication with aboveground devices in wireless underground sensor networks: An empirical study," in *2010 IEEE international conference on communications*. IEEE, 2010, pp. 1–6.

[151] http://www.freelinc.com/.
[152] http://ru-bee.com/.
[153] A. Markham and N. Trigoni, "Magneto-inductive networked rescue system (miners): Taking sensor networks underground," in *IPSN*, 2012, pp. 317–328.
[154] "Near-field magnetic induction for wireless audio and data streaming," https://www.futureelectronics.com/resources/get-connected/2017-06/future-electronics-near-field-magnetic-induction.
[155] X. Tan, Z. Sun, and I. F. Akyildiz, "Wireless underground sensor networks: Mi-based communication systems for underground applications." *IEEE Antennas and Propagation Magazine*, vol. 57, no. 4, pp. 74–87, 2015.
[156] U. Raza and A. Salam, "Zenneck waves in decision agriculture: An empirical verification and application in em-based underground wireless power transfer," *Smart Cities*, vol. 3, no. 2, pp. 308–340, 2020.
[157] S. Jiang, S. V. Georgakopoulos, and O. Jonah, "Rf power harvesting for underground sensors," in *Proceedings of the 2012 IEEE International Symposium on Antennas and Propagation*, 2012, pp. 1–2.
[158] A. A. Eteng, S. K. A. Rahim, and C. Y. Leow, "Wireless nonradiative energy transfer: Antenna performance enhancement techniques." *IEEE Antennas and Propagation Magazine*, vol. 57, no. 3, pp. 16–22, 2015.
[159] A. Karalis, J. D. Joannopoulos, and M. Soljacic, "Efficient wireless non-radiative mid-range energy transfer," *ANNALS OF PHYSICS*, vol. 323, 2006.
[160] A. Kurs, A. Karalis, R. Moffatt, J. D. Joannopoulos, P. Fisher, and M. Soljacic, "Wireless power transfer via strongly coupled magnetic resonances," *Science*, vol. 317, no. 5834, pp. 83–86, 2007.
[161] U. Raza and A. Salam, "On-site and external energy harvesting in underground wireless," *Electronics*, vol. 9, no. 4, 2020.
[162] S. Kahrobaee and M. C. Vuran, "Vibration energy harvesting for wireless underground sensor networks," in *IEEE ICC*, 2013, pp. 1543–1548.